

ЛАХРУД, ОСТАНЕЦ ПАЛЕОТЕТИСА В СЕВЕРО-ЗАПАДНОМ ИРАНЕ: ГЕОХИМИЧЕСКИЙ И РАДИОИЗОТОПНЫЙ СОСТАВ, ГЕОХРОНОЛОГИЯ И ТЕКТОНИЧЕСКАЯ ОБСТАНОВКА ОБРАЗОВАНИЯ

С. Хасанпур

Department of Geology, Payame Noor University, Iran

Офиолит Лахруд на северо-западе Ирана включает обширные зоны палеозойского офиолита, являющегося останцем океанической коры Палеотетиса. Основными его породами являются габбро, перекрытые подушечным базальтом, который прорван гранитами, переслаивающимися с пелагическими осадками, в том числе кремнистыми породами с радиолариями. Результаты геохимических и радиоизотопных исследований, а также данные по изотопии Nd, Sm, Sr и Pb указывают на то, что офиолит Лахруд возник из базальтовой лавы внутриплитного мантийного источника. Изотопные исследования показывают, что базальты являлись производными расплавов океанической мантии индийского типа. Радиогенные данные свидетельствуют о присутствии в исходной магме связанного с субдукцией терригенного материала. Все породы геохимически когенетичны и образовались в результате фракционирования расплава, имевшего средний состав E-MORB с известково-щелочной специализацией. $^{40}\text{Ar}/^{39}\text{Ar}$ возраст минералов мусковита и стекол (343 ± 3 и 187.7 ± 7.7 млн лет соответственно) указывает на то, что метаморфические и базальтовые породы сформировались в позднем палеозое и ранней юре соответственно. Результаты микрофоссильных исследований свидетельствуют о наличии в структуре офиолите палеозойских биостратиграфических подразделений. Кристаллизация и рифтообразование в океанической коре офиолита Лахруд начались, вероятно, в каменноугольном периоде; вулканическая активность здесь продолжалась в течение позднего триаса.

Лахруд, офиолит, Палеотетис, Азербайджан, Иран

LAHROUD, A PALEO-TETHYS REMNANT IN NORTHWESTERN IRAN: IMPLICATIONS FOR GEOCHEMISTRY, RADIOISOTOPE GEOCHRONOLOGY, AND TECTONIC SETTING

S. Hassanpour

The Lahroud Ophiolite in northwestern Iran contains extensive zones of Paleozoic ophiolite as remnants of the Paleo-Tethys oceanic crust. The principal rock units are gabbro overlain by pillow basalt, which is intruded by granites and interbedded with pelagic sedimentary units including radiolarian cherts. Geochemistry and radioisotope studies, supported by Nd, Sm, Sr, and Pb isotope data, indicate that the Lahroud Ophiolite originates from a within-plate basaltic mantle source. The isotope studies show that the basalts are derived from Indian-type oceanic mantle sources. The radiogenic data indicate the involvement of subduction-related terrigenous materials in the source magma. All the rocks are geochemically cogenetic and were generated by fractionation of a melt with a composition of average E-MORB with a calc-alkaline signature. Two $^{40}\text{Ar}/^{39}\text{Ar}$ ages, 343 ± 3 Ma for muscovite minerals and 187.7 ± 7.7 Ma for glasses, suggest that metamorphic and basaltic rocks formed during the Late Paleozoic to Early Jurassic, respectively. Microfossil studies show the presence of Paleozoic biostratigraphy. The crystallization process and rifting into the oceanic crust in the Lahroud Ophiolite probably began in the Carboniferous, with volcanic activity continuing during the late Triassic.

Ophiolite, Paleo-Tethys, Lahroud, Azerbaijan, Iran

INTRODUCTION

Oceanic lithosphere fragments remained as ophiolites and were accreted through orogenic phases. The present-day locations of the ophiolites represent a suture zone and are important markers in the reconstruction of the tectonic history (Dilek, 2003). A complete ophiolite typically comprises, from top to bottom: pillow lava, sheeted dikes, and cumulate mafic to ultramafic units (Anonymous, 1972). However, not all preserved ophiolites contain a complete sequence. Commonly, ophiolites are strongly deformed and metamorphosed during uplift. Iranian ophiolites and their locations are shown in Fig. 1 and were classified in several ways by different authors. Arvin and Robinson (1994) divided Iranian ophiolites into two groups based on their ages: Paleozoic ophiolites in the north of Iran (less common) and Mesozoic ophiolites (more common) in the south of Iran, near

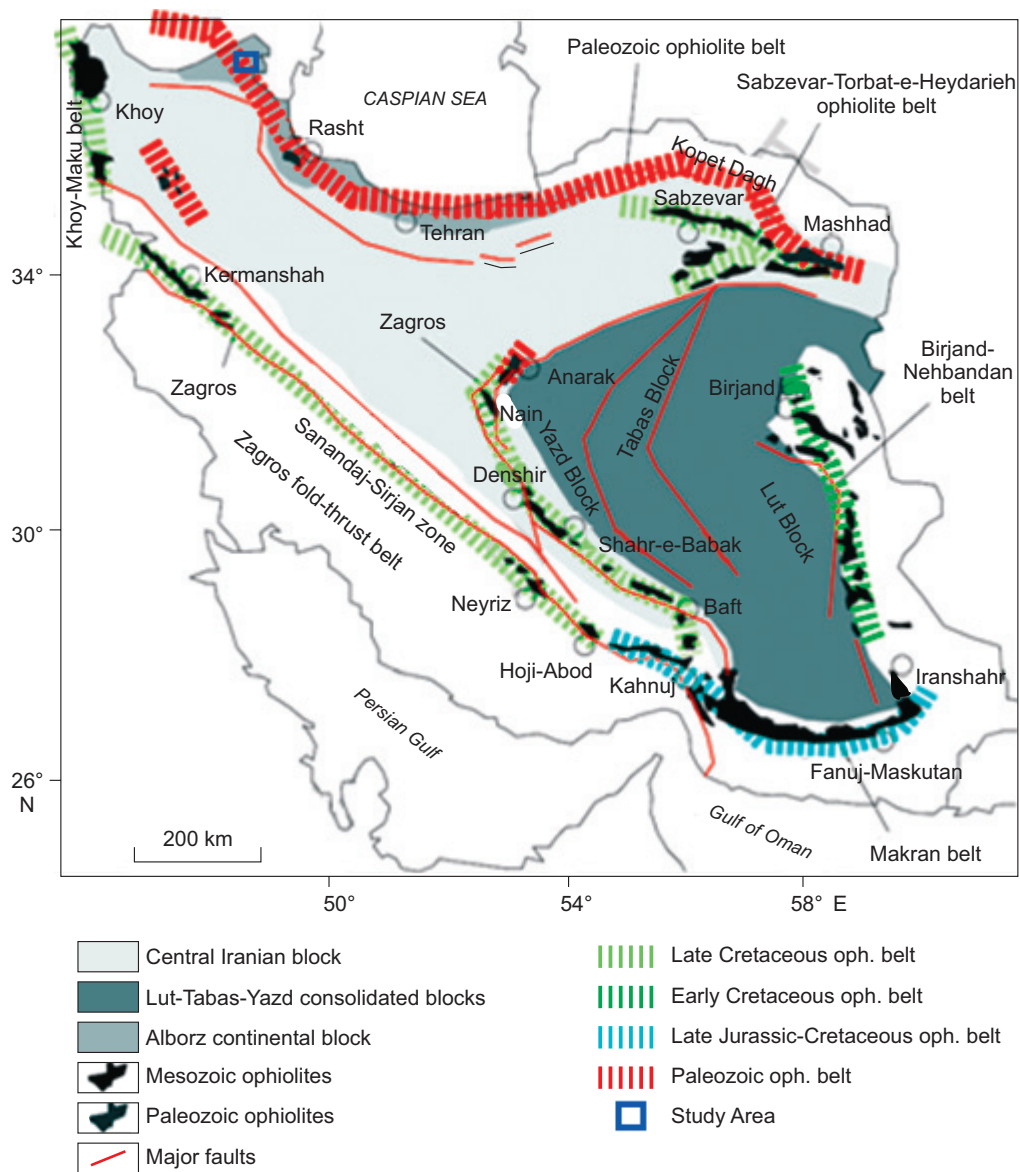


Fig. 1. Simplified regional geological map of Iran, emphasizing the main ophiolitic belts (thick dashed lines), modified from (Shafaii Moghadam et al., 2015a).

the main central Iranian block ophiolites (Shafaii Moghadam and Stern, 2011). Recently, Iranian ophiolites have been classified into four groups based on their location and geotectonic setting: (a) northern ophiolites along the Alborz range; (b) Zagros ophiolites as a suture zone; (c) unfragmented ophiolites in the Makran zone; and (d) Central Iranian Microcontinent (CIM) ophiolites and colored mélanges (Takin, 1972; Stöcklin, 1974; McCall, 1997) (Fig. 1, Table 1).

The CIM comprises the Lut, Posht Badam, Tabas, and Yazd ophiolites (Fig. 1, Table 1). Alavi (1991) classified Iranian ophiolites through observations of field relationships into three groups: (a) Proterozoic, which is presented on the western edge of the CIM as an isolated outcrop; (b) pre-Jurassic, which is located in the Alborz E–W Range; and (c) post-Jurassic, which is the most abundant. Table 1 shows the distributions, age, and tectonic settings of ophiolites in Iran (Ghazi et al., 2003). In Figure 1, the location of Paleo-Tethys ophiolites are traced in an east–west trend. These ophiolitic slices in the north of Iran are composed of Darrehanjir, Mashhad, Fariman (in Kopet Dagh), Jandagh–Anarak, Takab, and Rasht ophiolites (Fig. 1) (Shafaii Moghadam et al., 2015a).

Paleozoic ophiolites in the southwestern part of Asia are exposed in the Caucasus across Iran, Turkey (Küre mélangé), Turkmenistan, Afghanistan, and Tibet (Shi et al., 2012; Meng et al., 2013). The distribution of Paleozoic ophiolites along the southern margin of Eurasia represents the closure of the Paleo-Tethys oceanic basin (Stampfli and Borel, 2002; Bagheri and Stampfli, 2008; Rolland et al., 2011; Omrani et al., 2013; Zanchet-

Table 1. **Distribution of Iran ophiolites**

Region	Ophiolite Complex	Formation age, Ma	Emplacement age, Ma	References
N–NW	Khoy	154–159 (Ar/Ar)	106–110 (Ar/Ar) 143 (Muscovite)	(Ghazi et al., 1997a) (Hassanipak and Ghazi, 2000)
Zagros	Rasht	Pre-Jurassic	(?)	(Alavi, 1996)
	Kermanshah	95–98 (Ar/Ar) (?)	Post-Campanian Pre-Maastrichtian	(Lippard et al., 1986) (Ghazi and Hassanipak, 1999)
	Sahneh	86.3?	(?)	(Delaloye and Desmons, 1980)
	Neyriz	93–95 Ma (Ar/Ar)	89 Ma (Ar/Ar)	(Lanphere and Pamić, 1983; Sarkarinejad, 1994; Ghazi et al., 1999)
		96–98 Ma (Ar/Ar)	Post-Campanian Pre-Maastrichtian	
South–Central	Nain	93–95 Ma (Ar/Ar)	Pre-Paleocene	(Lippard et al., 1986; Sarkarinejad, 1994; Hassanipak and Ghazi, 2000)
	Shahr-e-Babak	93 Ma (Ar/Ar)	Pre-Paleocene	(Aftabi and Fathi, 1992; Campbell et al., 2000; Tucker et al., 2000)
	Baft–Esphandagheh	Upper Cretaceous	Pre-Paleocene	
Makran	Band-e-Zeyarat	140–142 (Ar/Ar)	Early Paleocene	(Desmons and Beccaluva, 1983; Hassanipak et al., 1996; Ghazi et al., 1997b; McCall, 1997; Ghazi et al., 1999)
	Dar Anar			
	Ganj	135 K/Ar	Early Eocene	(McCall, 1985)
	Remeshk/Mokhtar	Late Jurassic–	Early Paleocene	(Desmons and Beccaluva, 1983; McCall, 1985; Hassanipak et al., 1996; McCall, 1997)
	Abad	Early Cretaceous		
	Iranshahr	Upper Cretaceous	Pre-Paleocene	
	Fanuj–Maskutan	Upper Cretaceous	Pre-Paleocene	
		Upper Cretaceous		
East–North-east	Tchehel-Kureh	Upper Cretaceous	Pre-Paleocene	(Delaloye and Desmons, 1980; Desmons and Beccaluva, 1983; Lippard et al., 1986)
	Sabzevar	52.4 (Ar/Ar)	Post-Paleocene	(Lensch et al., 1977; Lensch, 1980; Shojaat, 1999; Hassanipak et al., 2002)
	Mashhad	277–281 (Ar/Ar)	Pre-Jurassic	(Alavi, 1992, 1996; Ghazi et al., 1999; Hassanipak et al., 2002)
NW	Lahroud (Allahyarlou)	245–187 Ma (Ar/Ar)	Paleozoic	This study

ta et al., 2013). In the southern part of Eurasia, the Paleo-Tethys Ocean formed during the Late Paleozoic. Closure of the Paleo-Tethys commenced in the Middle to Late Jurassic (the Eo-Cimmerian deformation (Boulin, 1988; Zanchi et al., 2009)), resulting in the formation of modern northern Iran and Afghanistan. The Paleo-Tethys rifting produced alkali–tholeiitic continental flood-type basalts (Soltan-Meidan basalts), felsic to mafic plutonic rocks (ages of ca. 460 Ma) (Shafaii Moghadam and Stern, 2011), dolomite, evaporites, and terrigenous sediments in the Ordovician (Ghelli) and Lower Devonian (Padeha) formations in the northern part of Iran (Stampfli, 1978; Aharipour et al., 2010). Studies showed that, following Ordovician to Silurian rifting, seafloor spreading of the Paleo-Tethys was diachronous and varied from Devonian to Permian. Prior to this study, the age of closure of the Paleo-Tethys in northwestern Iran was (in the east–west trend) unknown. This paper presents the results of studies on the formation and evolution of the Lahroud (Allahyarlou) ophiolite in northwestern Iran, including petrographic studies, chemical and isotope analyses, field observations, and radiometric age dating. Based on the results, the stratigraphy, igneous-rock composition, and petrogenesis were determined to discuss the tectonic and biostratigraphic setting of the ophiolite in the context of the closure of the Paleo-Tethys Ocean.

REGIONAL GEOLOGY

The Lahroud area in the northwestern part of Iran is a relatively small, very poorly known outcrop that is situated in the Alborz zone (Stöcklin, 1968; Berberian et al., 1981) and the southern part of the Caspian depression. The Lahroud ophiolite is a part of several ophiolite outcrops in northeastern Iran. All of some ophiolitic patches are distributed tectonically at the boundary between the CIM and the Alborz Mountains in an east–west

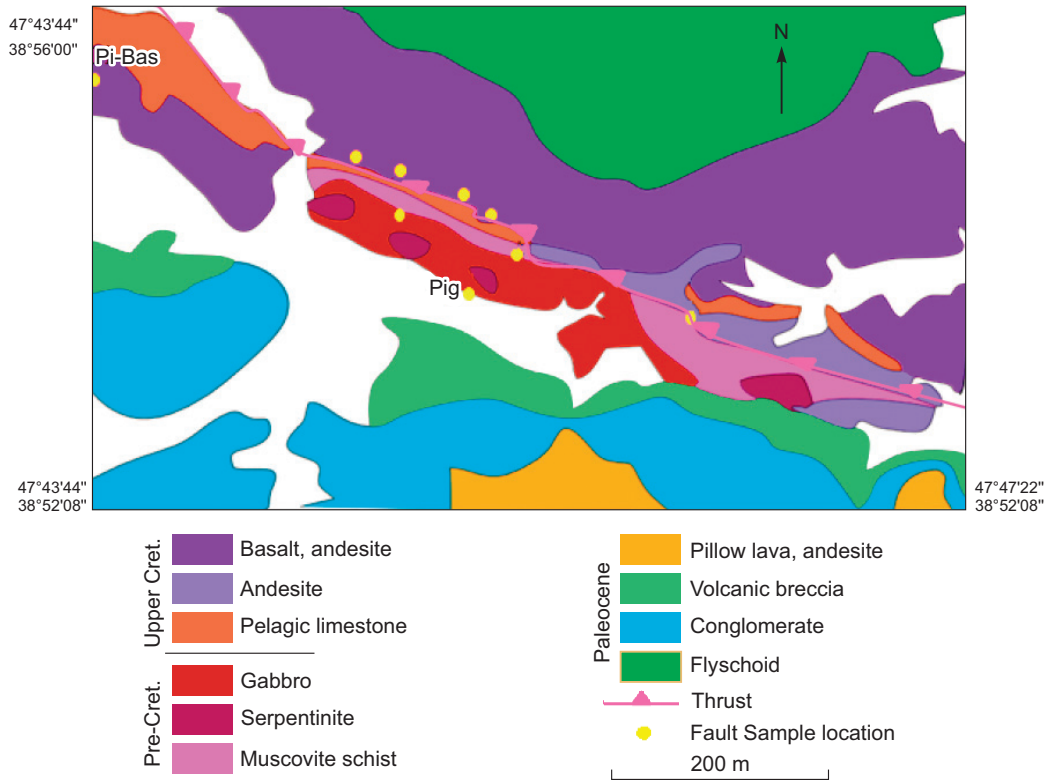


Fig. 2. Simplified local geological map of the ophiolitic sequence in the Lahroud area (Fig. 3) with sample locations, after (Amidi et al., 1991).

trend among Gondwana and Eurasian plates (Paleo-Tethys suture zone). This ophiolite is considered to be a part of the northern branch of the Paleo-Tethys Ocean that opened and closed during the Paleozoic and Early Jurassic, and it might be related to the ophiolites of the Lesser Caucasus.

In the Lahroud (Alahyarlou) area, three important regional geologic features are distinguished: (a) the Lahroud ophiolite sequence, which is composed of gabbro and ultramafic rocks and unconformably overlain by (b) Upper Jurassic to Cretaceous pillow lava not from the ophiolite sequence, which overlies ophiolitic sequences; and (c) pelagic limestones in some patches in the region and around the sequences (Figs. 2, 3). The Lahroud sequence comprises gneiss, amphibolite, chlorite schist, and metadiabase that are associated with serpentinites, gabbro, dunite, tectonic breccia, and marbles. The complex has an ultramafic–gabbroic unit containing some sequences of gabbroic rock units that are preserved and overlain by sheeted diabase dikes. Other dikes which strike parallel to the ophiolite are also observed (Fig. 2). The Lahroud sequence is weakly serpentinitized. The pelagic limestone strike is east–west. Pelagic limestones are pink and red in color with intercalation of yellow and greenish shale and marl. Thin layered limestones are oolitic, especially in the upper parts, and are white to red in color, with fossils of Late Paleozoic age. It seems to be in relation to Sevan–Aker (Berberian et al., 1981). As a whole, the Lahroud Complex is cut by two fault systems: the Angot Fault complex with a NW–SE trend and the Alahyarlou Fault in the west with a north–south trend (Fig. 2).

PETROGRAPHY

Intrusive rocks. Plutonic rocks of the Lahroud ophiolite are exposed in the area. They are composed of mafic to ultramafic rock units, with ultramafic rocks comprising nearly two-thirds of the entire ophiolite complex. The crustal sequence consists largely of gabbro, which is present as relatively small bodies, and appears to be fragmented parts of tectonically dismembered large units. For the purpose of the study and according to the geochemistry and metamorphic degree, it is divided into metagabbro and younger gabbro units. Metagabbro, which is mainly cumulate-banded gabbro, comprises porphyroclasts of plagioclase (60 to 70%), pyroxene (30 to 40%), and amphiboles (0 to 5%) with intergranular and interstitial textures (Fig. 4a). Some of the rocks show degrees of alteration that are partly pervasive. This unit is also affected by metamorphic events (amphibole–mus-

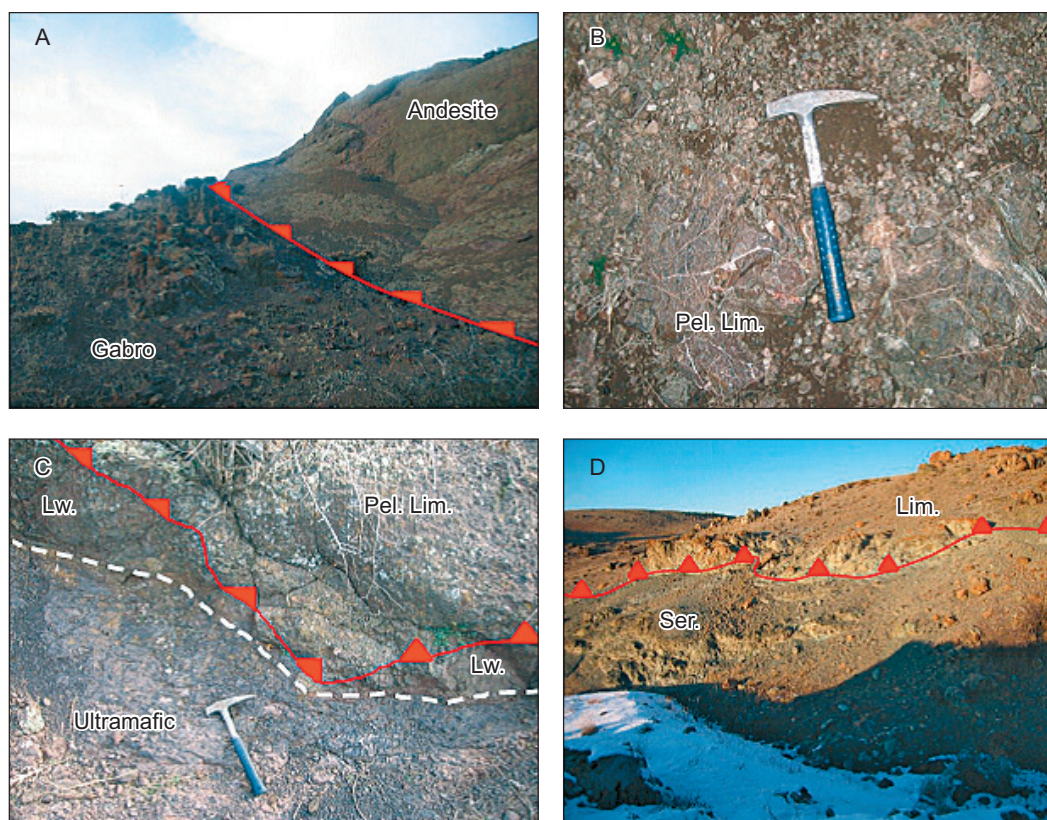


Fig. 3. Photographs of rock units in the Lahroud area. Post-Paleozoic limestone overlies an ophiolitic association, gabbro, an ultramafic unit, pillow lavas, and serpentinites.

a, The gabbro is overthrust by a younger andesite to basaltic andesite unit (Cretaceous); *b*, Paleozoic pelagic limestone; *c*, pelagic limestone on gabbro and ultramafic units with partly listwänite patches orange in color, a tectonized contact, and hydrothermal alteration effects; *d*, limestones overthrust on the serpentinites. Pel. lim., Pelagic limestone; Lw., listwänite; Lim., limestone; Serp., serpentinite.

covite schist). Amphibolite has been dated (Fig. 4*a, b*), and the results are described in this research. This crustal sequence consists of gabbro that is presented as a small body and appears as fragments of tectonically larger units (Fig. 4*c*). Most of these rocks exhibit some degree of serpentinization, which is locally pervasive.

The younger gabbro in the area is fresher and is largely composed of noncumulate rocks with ophitic textures. It has partly small outcrops in the western part of the region and is formed in the sequence consisting of porphyroclasts of plagioclase (60 to 70%), pyroxene (30 to 40%), and amphiboles (0 to 5%) with intergranular or interstitial textures. Pyroxene and plagioclase phynocrysts show ophitic texture (Fig. 4*d*). This gabbro is, respectively, fresher than the old gabbro except for very thin calcifications.

Extrusive rock units. Extrusive rocks in the Lahroud ophiolite occur as massive, coherent bodies and rarely as pillow lavas. Most of the basalts, andesite, basaltic andesite, and pillow lavas are altered to some extent, but relict igneous textures are well preserved. In most areas, the pillow lavas are intercalated with a mixture of lava clasts, shallow- and deep-water fossiliferous limestone clasts, and reddish clasts of jasper and chert. These blocks of limestone and cherts vary in size from a few meters to tens of meters.

In hand specimen, these rocks are largely aphyric and contain microvesicles that are filled with zeolite and carbonate. Studies under microscope show largely aphyric textures (Fig. 4*e*). Andesite and basaltic andesite contains phenocrysts of plagioclase occurring alone or as clusters of closely packed crystals in a matrix of plagioclase microlites. The majority of these rocks are porphyritic, containing phenocrysts of plagioclase and hornblende and to a lesser extent clinopyroxene in a fine-grained matrix. Basalts in the region are mostly spilitic at the surface.

In the upper part of the area, the pillow lavas are overlain by deep-water fossiliferous limestones. This block of a limestone unit and cherts varies in thickness from a few meters to some ten meters and is interbedded with reddish jasper and cherts.



Fig. 4. Photomicrographs (cross-polarized light) of metamorphic rocks.

a, Amphibolite, the oldest rock with amphiboles that have been dated; *b*, *c*, metagabbro with phenocrysts of pyroxene and micas; *d*, freshest gabbro in the area as the above part of the complex; *e*, basalt, spilite; *f*, metamorphosed rocks, muscovite–sillimanite schist; *g*, serpentinite with a large amount of talc; *h*, serpentinite in hand specimen; *i*, amphibole and muscovite in metamorphosed rock. Amph, Amphibole; Talc, talc; Plag, plagioclase; Bio, biotite; Pyrox, pyroxene; Horn, hornblende; Ol, olivine; Sil, sillimanite; Mus, Muscovite; Serp, serpentinite.

METAMORPHISM

The old rocks from the mafic units in the ophiolite sequence are metamorphosed. Amphibolite, muscovite schist, and sillimanite schists are the major features which are observed in the region. Metamorphic rocks comprise schist with porphyroblasts of muscovite and sillimanite as the major phenocrysts (Fig. 4*f*).

The mafic rocks are mostly converted to serpentinite. It also has remarkably green and talcous outcrops in the area (Fig. 4*g*, *h*).

Silica–carbonates (listwänites). Listwänites form as a result of the chemical reaction between serpentinite and CO₂-rich fluids. These fluids usually migrate along faults or fractures along the contact of serpentinite and the adjacent country rocks in the region. Freshly broken listwänites have a green–orange color, and the weathered surface of listwänites shows gossanous boxwork texture and a brown–red color owing to the preferential breakdown of the ferro-magnesium carbonates (Fig. 3*c*). Silica–carbonates in the Lahroud region commonly contain chlorite, talc, and residual serpentine without chromite- or mineralization-bearing of any sulfides.

ANALYTICAL METHODS

ICP MS and ICP OES. Seven samples were pulped for analysis of major and trace elements, including rare-earth elements (REE), by fusion inductively coupled plasma mass spectroscopy and inductively coupled plasma optical emission spectroscopy (ICP MS and ICP OES) at Amdel in Australia. The detection limit was 0.01% for all major element oxides and 0.5–1 ppm for rare-earth elements. The representative major- and trace-element compositions of the Lahroud rocks are presented below.

Ar–Ar dating. Two samples of muscovite and glass minerals (about 40–50 grains per sample) were prepared from representative samples from the basalt unit and metamorphosed rock in Lahroud, following crushing, washing, and handpicking under the binocular microscope.

Muscovite (200–300 μm) from sample OPh15, representing the metamorphosed rock, and concentrates from sample OPh7, also from the basalt unit, was prepared. The freshest samples were used in this regard. The mineral separates were wrapped in aluminum foil and stacked in an irradiation capsule with similar-aged samples and neutron flux monitors (Fish Canyon Tuff sanidine (FCs), 28.02 Ma (Renne et al., 1998)). The samples were irradiated at the McMaster Nuclear Reactor in Hamilton, Ontario, for 43 MWh, with a neutron flux of approximately 6×10^{13} neutrons/cm²s. Analyses ($n = 30$) of six neutron flux monitor positions produced errors of <0.5% in the J values.

The samples were analyzed at the Noble Gas Laboratory, Pacific Centre for Isotopic and Geochemical Research (PCIGR), University of British Columbia (Vancouver). The mineral separates were step-heated at incrementally higher powers in the defocused beam of a 10W CO₂ laser (New Wave Research MIR10) until fused. The gas evolved from each step was analyzed by a VG5400 mass spectrometer equipped with an ion-counting electron multiplier. All measurements were corrected for total system blank, mass spectrometer sensitivity, mass discrimination, radioactive decay during and subsequent to irradiation, and interfering Ar from atmospheric contamination and the irradiation of Ca, Cl, and K (isotope production ratios: $(^{40}\text{Ar}/^{39}\text{Ar})\text{K} = 0.0302 \pm 0.00006$, $(^{37}\text{Ar}/^{39}\text{Ar})\text{Ca} = 1416.4 \pm \pm 0.5$, $(^{36}\text{Ar}/^{39}\text{Ar})\text{Ca} = 0.3952 \pm 0.0004$, $\text{Ca}/\text{K} = 1.83 \pm 0.01$ ($(^{37}\text{ArCa}/^{39}\text{ArK})$)).

In general, total gas ages, plateau ages, and inverse isochron ages are concordant within 2σ error, which rules out major problems caused by either excess argon or partial argon loss (Table 3).

Radiogenic isotopes (Rb, Sr, Sm, Nd, and Pb). All the rocks in the study area were subjected to moderate to intense alteration. It is impossible to find reasonably fresh igneous rocks in outcrop. Our studies were carried out on one sample whole-rock analyses of basaltic rock (pillow lava). This sample, in addition to the other six samples, was analyzed litho-geochemically as noted above. The sample (basalt) as a whole rock after crushing and powdering was prepared for isotopic measurements following the procedure at the University of British Columbia. Isotopic ratios of Nd, Pb, and Sr and isotope-dilution abundances of Nd, Sm, Pb, Th, U, Sr, and Rb were measured at the University of British Columbia, PCIGR (Table 4).

GEOCHEMISTRY

The samples in the research were analyzed using the methods that mentioned above. Eight rock samples from the Lahroud region were analyzed (Table 2). The samples show a variable composition. The SiO₂ content of the Lahroud ophiolite ranges from 41 to 55 wt.%. The Mg# ($\text{Mg}/(\text{Mg} + \text{Fe}^{2+})$ molar ratio, assuming $\text{Fe}^{2+} = 0.9(\text{Fe})$ total given as Fe₂O₃ in Table 2) of the Lahroud samples are 0.8–4.5 wt.%. In addition, the samples from the Lahroud ophiolite contain TiO₂ (0.08–1.3 wt.%). The granite has a low aluminum content. Al₂O₃ contents are 12.5 wt.%, but SiO₂ contents are high, almost 77 wt.%. However, unlike the other oceanic granites that show low contents of K₂O (4.4 wt.%), the sample from Lahroud has a high K₂O content. Pillow basalt from the complex shows a calc-alkaline affinity and contains less than 2% K₂O, which characterizes the basaltic samples as ophiolitic. Besides their moderate LOI (~0.06–5%), the basaltic rocks are more extensively altered, because of ocean floor hydrothermal activities and later metamorphism. Thereby, we used trace elements because of their relative immobility via hydrothermal alteration processes and low-grade metamorphic conditions (e.g., Ta, Hf, Ti, Nb, Y, and Zr) in characterizing the basalts. The Lahroud rocks are trachyandesite, andesite, basalt, and andesitic basalt. Using the Zr/Y–Zr discriminant diagram, there is a clear distinction between basalts plotted within in the plate fields. Based on the AFM plot (Fig. 5a), all the samples show the calc-alkaline series (Irvine and Baragar, 1971). Based on (Meschede, 1986), the Zr–Nb–Y discrimination diagram illustrated that extrusive rocks plotted in four type fields. Andesite, andesite basalts, and basalts show calc-alkaline chemical affinities (Fig. 5b). The pattern for basalts, based on chemical analysis, is divided into two groups: within-plate alkaline basalt (AII) and within-plate tholeiite and within-plate tholeiites and volcanic-arc basalts (c). We used discrimination diagrams (Wood, 1980) to compare the geochemical characteristics for basalts in ternary diagrams like Th–Nb–Hf. The Lahroud basalts plot as D-type destructive plate-margin basalt and are differentiated from the original basaltic melt. Meanwhile, on the diagram (Th–Nb–Hf), all the samples illustrate a slight depletion in Nb (Fig. 5c). The ratios of Nb/Y and Zr/Y for pillow lava samples range from 0.21 to 1.18 and from 4.1 to 6.1, respectively (Table 5).

REE geochemistry. Table 2 lists REE analysis results, and Fig. 5d, e, show the chondrite-normalized REE patterns for samples of the entire sequence of rocks in the crustal section of the Lahroud ophiolite, representing the igneous stratigraphy of the ophiolite and the overall range of REE abundances. In Fig. 5d, e, the REE patterns for rocks from gabbro and metagabbro units are shown (Oph 22, 21, and 15 are ultramafics; Oph 7 and 4 and Pi-bas are basalts, and Plgr are granite rocks).

Table 2. **Bulk rock geochemical analyses of selected samples from the Lahroud ophiolite**

Sample	SiO ₂	TiO ₂	Al ₂ O ₃	Fe ₂ O ₃ **	FeO**	MnO	MgO	CaO	Na ₂ O	K ₂ O	P ₂ O ₅	LOI	Total	
Unit	wt.%	wt.%	wt.%	wt.%	wt.%	wt.%	wt.%	wt.%	wt.%	wt.%	wt.%	wt.%	wt.%	
Oph15	41.53	1.017	16.09	2.29	6.364	0.19	12.7	12.6	0.229	0.16	0.08	3.53	97.5	
Oph17	44.99	2.199	13.99	4.2	4.691	0.23	2.31	10.2	5.341	2.32	0.89	5.74	97.1	
Oph21	49.57	1.818	16.18	4.1	5.114	0.16	5.87	5.93	4.192	2.05	0.3	3.46	99.5	
Oph22	52.56	1.051	15.98	3.11	5.303	0.18	5.79	7.16	2.965	2.49	0.27	2.32	99.9	
Oph4	53.87	1.367	17.15	4.49	5.127	0.14	2.92	4.59	7.319	0.2	0.39	2.72	101.1	
Oph7	45.77	2.268	14.43	3.91	4.743	0.22	2.17	9.86	5.297	2.16	0.96	7.74	98	
Pi-BAS	55.32	1.317	15.65	3.5	5.48	0.17	4.44	4.74	3.397	1.62	0.26	4.28	100	
Plgr	77.08	0.083	12.5	0.83	0.664	0.01	0.12	0.13	3.572	4.42	0.009	0.62	100	
Sample	Ba	Rb	Sr	Cs	Li	Tl	Nb	Hf	Zr	Y	Th	U	Cr	
Unit	ppm	ppm	ppm	ppm	ppm	ppm	ppm	ppm	ppm	ppm	ppm	ppm	ppm	
Oph15	38.8	4.8	423	0.6	105	<0.1	1.5	0.7	24	24.4	0.3	<0.1	50	
Oph17	282	41.7	398	0.9	12	0.1	49.1	4.3	329	39.7	5.9	1.4	<50	
Oph21	226	53.6	390	0.9	29	0.3	17.5	3.8	183	23.7	2.7	0.9	100	
Oph22	1280	72.8	500	1	19	0.3	10	0.6	17	20.2	3.7	0.9	100	
Oph4	46.7	2.8	215	<0.1	7	<0.1	13	4	186	34.1	2.6	0.7	<50	
Oph7	424	39.4	387	1.2	13	0.1	47.5	5.1	248	40.2	6	1.6	<50	
Pi-BAS	158	36.6	209	1.1	18	0.2	7	3.5	137	32.9	1.8	0.5	<50	
Plgr	323	132	97	1	6.5	0.9	11.5	5	141	31.1	22.2	6.7	<50	
Sample	Ni	Co	Sc	V	Cu	Pb	Zn	Bi	Cd	Sn	W	Mo	B	Be
Unit	ppm	ppm	ppm	ppm	ppm	ppm	ppm	ppm	ppm	ppm	ppm	ppm	ppm	ppm
Oph15	141	37.6	38.5	285	283	1	54	<0.1	<0.5	<1	0.5	<0.5	<5	0.2
Oph17	11	19.2	11.8	133	22	5	144	<0.1	<0.5	5	<0.5	1	<5	0.7
Oph21	65	34.8	23	180	60	3	98	<0.1	<0.5	<1	<0.5	1	<5	1.3
Oph22	41	31.1	27.5	200	12	17	92	<0.1	<0.5	<1	<0.5	<0.5	<5	1.3
Oph4	<1	16	17	95	16	3	87	<0.1	<0.5	1	<0.5	0.5	<5	0.8
Oph7	7	23.1	12.5	120	15	8	120	<0.1	<0.5	2	<0.5	2	<5	0.9
Pi-BAS	16	24	29	160	40	4	103	<0.1	<0.5	1	<0.5	0.5	<5	0.6
Plgr	6	1.6	2.5	<5	6	10	24	0.2	<0.5	3	2	4	<5	1.8
Sample	Ag	Re	S	As	Sb	Te	La	Ce	Pr	Nd	Sm	Eu	Gd	Tb
Unit	ppm	ppm	ppm	ppm	ppm	ppm	ppm	ppm	ppm	ppm	ppm	ppm	ppm	ppm
Oph15	<0.1	<0.1	150	<1	<0.2	<0.2	2.9	8.2	1.2	6.18	2.2	0.78	3	0.52
Oph17	<0.1	<0.1	173	9	0.2	<0.2	39.9	81.1	10.02	42.01	7.99	2.97	7.87	1.27
Oph21	<0.1	<0.1	200	2	0.2	<0.2	22.3	46.8	5.6	22.2	4.8	1.58	4.45	0.64
Oph22	<0.1	<0.1	50	5	1	<0.2	24.3	46.1	6.2	23.1	4.78	1.6	4.6	0.64
Oph4	<0.1	<0.1	<50	<1	<0.2	<0.2	19.5	40.1	5.25	21.7	5.46	1.94	5.45	0.86
Oph7	<0.1	<0.1	250	5	0.2	<0.2	40.6	79.1	9.75	38.4	8.58	3.12	8.05	1.22
Pi-BAS	<0.1	<0.1	50	4	<0.2	<0.2	12.7	26.4	3.85	16.9	4.86	1.66	5.3	0.86
Plgr	<0.1	<0.1	50	6	1.2	<0.2	45	83.9	9.75	34.2	7.04	0.7	5.8	0.98
Sample	Dy	Ho	Er	Tm	Yb	Lu	Ge	Nb/Y	Zr/Y	La/Sm	Th/Nb	Nb/Yb	Th/Yb	
Unit	ppm	ppm	ppm	ppm	ppm	ppm	ppm	ppm	ppm	ppm	ppm	ppm	ppm	
Oph15	3.66	0.8	2.35	0.35	2.2	0.32	<0.5	0.06	0.98	1.31	0.2	0.682	0.14	
Oph17	7.45	1.32	3.73	0.5	3.22	0.5	<0.5	1.48	8.28	4.99	0.12	15.24	1.83	
Oph21	3.88	0.76	2.05	0.3	1.75	0.26	<0.5	0.73	7.72	4.64	0.15	10	1.54	
Oph22	3.82	0.78	2.05	0.3	1.85	0.28	<0.5	0.49	0.84	5.08	0.37	5.41	2	
Oph4	5.88	1.14	3.2	0.45	3.05	0.48	<0.5	0.38	5.45	3.57	0.2	4.3	0.85	
Oph7	7.84	1.46	3.85	0.55	3.35	0.5	<0.5	1.18	6.16	4.73	0.13	14.2	1.79	
Pi-BAS	6.02	1.16	3.35	0.45	3.05	0.46	<0.5	0.21	4.16	2.61	0.26	2.3	0.59	
Plgr	6.16	1.28	3.8	0.6	4.1	0.56	<0.5	0.36	4.53	6.39	1.93	2.8	5.42	

Table 3.

Ar–Ar age data

Sample SH175, glass													
Power, W	⁴⁰ Ar/ ³⁹ Ar	1s	³⁷ Ar/ ³⁹ Ar	1s	³⁶ Ar/ ³⁹ Ar	1s	Ca/K	Cl/K	% ⁴⁰ Ar atm	f ³⁹ Ar	⁴⁰ Ar*/ ³⁹ ArK	2s	Age
2.00	1196.37	17.80	9.89	0.35	4.121	0.107	18.24	–	101.71	0.31	20.646	–209.67	±560.55
2.20	765.79	6.27	8.76	0.26	2.641	0.059	16.14	–	101.81	0.95	13.982	–139.30	±341.21
2.30	275.92	5.76	19.26	0.72	0.941	0.028	35.75	–	100.16	0.51	0.439	–4.22	±120.86
2.60	35.21	0.28	72.69	1.34	0.094	0.002	140.33	–	61.57	3.29	14.263	131.83	±12.00
3.30	36.99	0.22	130.19	2.28	0.104	0.002	262.57	–	54.50	5.81	18.536	169.53	±13.86
4.00	24.84	0.14	90.18	1.64	0.052	0.001	176.39	–	32.10	12.40	18.013	164.96	±7.03
4.70	21.08	0.11	11.75	0.21	0.006	0.000	21.70	–	4.36	47.76	20.335	185.16	±1.98
5.00	22.34	0.12	8.55	0.15	0.006	0.000	15.76	–	4.25	20.05	21.520	195.39	±2.11
5.30	23.86	0.16	19.98	0.38	0.014	0.001	37.12	–	10.78	5.24	21.592	196.01	±4.23
5.90	25.45	0.19	0.21	0.02	0.014	0.001	0.38	–	16.75	3.06	21.189	192.54	±4.11
6.70	40.22	0.42	0.51	0.06	0.077	0.004	0.93	–	56.60	0.63	17.462	160.13	±19.03
Total/Average	24.738	0.056	0.475	0.015	0.0071	0.0001	–	–	–	100.00	20.765	0.073	

$$J = 0.0053024 \pm 0.0000265$$

$$\text{Volume } ^{39}\text{ArK} = 0.495$$

$$\text{Integrated date} = 188.97 \pm 1.26 \text{ Ma}$$

Plateau age = not defined

Inverse isochron (correlation age) results, plateau steps: Model 1 Solution ($\pm 95\%$ -conf.) on 11 points

$$\text{Age} = 190.3 \pm 6.5 \text{ Ma}$$

$$40/36 \text{ intercept: } 271 \pm 29 \text{ MSWD} = 20, \text{ Probability} = 0 \text{ (at } J=0.00530242 \pm 0.3\% \text{ } 2\sigma)$$

Sample SH179, muscovite

2.00	524.31	90.58	4.84	3.70	0.720	0.260	8.89	–	40.46	0.06	313.218	1724.71	±616.35
2.20	109.49	3.56	10.72	1.14	0.186	0.045	19.78	–	49.33	0.32	55.898	453.07	±192.83
2.50	109.74	1.64	11.60	0.39	0.251	0.007	21.43	–	66.83	2.99	36.707	309.96	±32.81
2.90	49.58	0.38	22.61	0.42	0.048	0.001	42.08	–	24.87	26.69	37.855	318.85	±6.93
3.50	42.65	0.25	8.49	0.16	0.007	0.000	15.64	–	3.09	63.06	41.578	347.38	±3.87
4.30	47.53	0.74	31.94	0.72	0.035	0.003	59.85	–	16.47	4.51	40.615	340.04	±16.24
5.30	48.82	0.60	32.91	1.16	0.015	0.005	61.71	–	3.39	2.37	48.293	397.71	±25.67
Total/Average	46.355	0.188	11.464	0.134	0.0088	0.0002	–	–	–	100.00	40.748	0.214	

$$J = 0.0050938 \pm 0.0000255$$

$$\text{Volume } ^{39}\text{ArK} = 0.052$$

$$\text{Integrated date} = 341.15 \pm 4.66$$

$$\text{Plateau age} = 347.0 \pm 4.9 \text{ Ma}$$

(2s, including J -error of 0.3%), MSWD = 0.77, 67.6% of the ³⁹Ar, steps 5 through 6

Inverse isochron (correlation age) results, plateau steps: Model 1 Solution ($\pm 95\%$ -conf.) on 7 points

$$\text{Age} = 344 \pm 18 \text{ Ma}$$

$$40/36 \text{ intercept: } 269 \pm 69 \text{ MSWD} = 15, \text{ Probability} = 0 \text{ (at } J=0.0050938 \pm 0.3\% \text{ } 2\sigma)$$

Note. Total fusion age, isochron age, inverse isochron age, and plateau age. All the errors are 2σ .

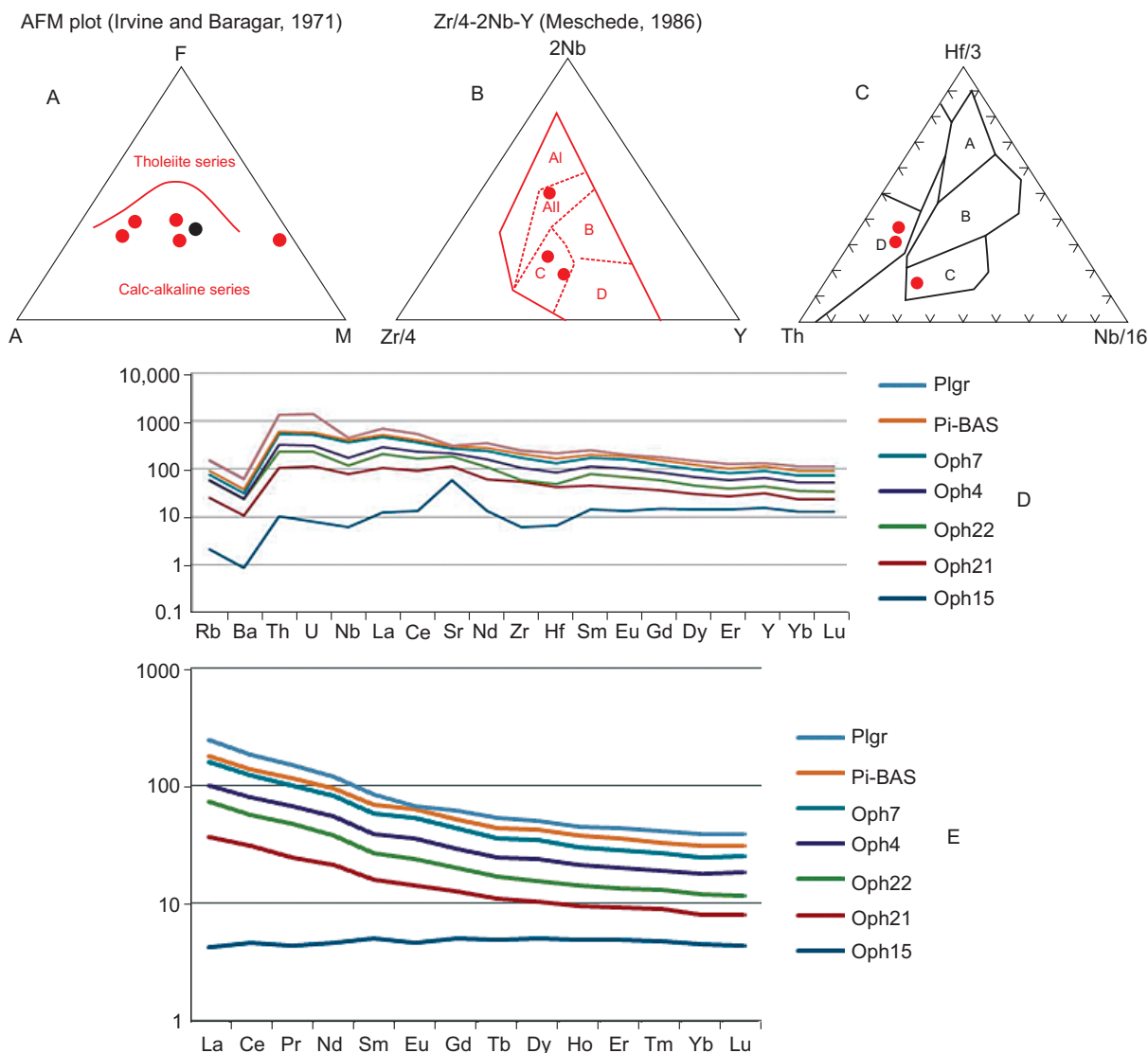


Fig. 5. AFM plot from (Irvine and Baragar, 1971)

a, all samples plotted in the calc-alkaline area; *b*, Nb–Zr–Y geochemical discrimination diagram (Meschede, 1986) showing two types of basaltic rocks: AI, WPA (within-plate alkaline basalts); AII, WPT (within-plate tholeiite); B, P-MORB (mid-ocean-ridge basalt); C–D, VAB (volcanic-arc basalt); *c*, Th–Hf–Nb discrimination diagram (Wood, 1980) showing that the basalt data plot in the compositional field of (A) N-MORB type, (B) B-MORB type and tholeiitic basalt within-plate and differentiates, (C) alkaline within-plate basalt and within-plate basalts and differentiates, and (D) destructive plate-margin basalts and differentiates. Samples from Lahroud fall into the D area; destructive plate-margin basalts and differentiates. *d*, Chondrite-normalized incompatible trace-element diagram for the rocks from the Lahroud ophiolite. Normalizing values for chondrite are from (Sun and McDonough, 1989). *e*, Chondrite-normalized REE patterns for (Oph 22, 21, and 15) low- and high-level gabbro, (Oph 7 and 4 and Pi-bas) basalt and diabbases, and (Plgr) granite. Normalizing values for chondrite are from (Sun and McDonough, 1989).

The gabbro has 100–150 chondrite concentrations of REE, and the patterns are characterized by enrichment in the light REE ((LaN/SmN)_{ave} = 0.81, where N means chondrite-normalized) and a very slight enrichment in the middle REE. Their primary mineralogy consists of hornblende and, to a lesser extent, plagioclase. The overall concentrations of MREE in the gabbro are slightly higher (~10 chondrite); however, they have also smaller positive Eu anomalies ((Eu/Eu*)_{ave} = 1.32). At the same time, for the only metagabbro sample, the REE pattern has a plateau with a slight enrichment in REE and with a chondrite-like feature. The REE patterns for the basalt samples are shown in Fig. 5e. The volcanic rocks are characterized by moderate REE enrichment ((LaN/SmN)_{ave} = 3.3) and positive Eu anomalies ((Eu/Eu*)_{ave} = 1.6). The REE pattern for basalt samples is similar in shape to patterns of the rest of the intrusive-rock samples (Fig. 5e). The REE patterns of the basalt samples from Lahroud are distinctly different from the patterns for diabbase samples from complex of the Mash-

Table 5.

**Incompatible trace element ratios in crust and mantle reservoirs
(from compilations by Saunders et al., 1988; Weaver, 1991)**

	Primitive mantle	N-MORB	E-MORB	Continental crust	HIMU-OIB	EMI-OIB	EMII	Lahroud
Zr/Nb	14.8	30		16.2	3.2–5.0	4.2–11.5	4.5–3	1.7–16.0
La/Nb	0.94	1.07		2.2	0.66–0.77	0.86–1.19	0.89–1.09	0.8–1.9
Ba/Nb	9	1.7–8.0	4.9–8.5	54	4.9–6.9	11.4–17.8	7.3–13.3	3.5–22.0
Ba/Th	77	6		124	49–77	103–154	67–84	14–129
Rb/Nb	0.91	0.36	205–230	4.7	0.35–0.38	0.88–1.17	0.59–0.85	0.2–7.0
K/Nb	323	210–350	0.06–0.08	1341	77–179	213–432	248–378	0.01–0.19
Th/Nb	0.117	0.025–0.071		0.44	0.078–0.101	0.105–0.122	0.111–0.157	0.2–0.25
Th/La	0.125	0.067		0.204	0.107–0.133	0.107–0.128	0.122–0.163	0.10–0.14
Ba/La	9.6	4		25	6.8–8.7	13.2–16.9	8.3–11.3	2.3–13.37

had ophiolites (Shafaii Moghadam et al., 2015a) and from the sequence pillow lavas. The REE patterns of basalts from the Mashhad ophiolites are depleted in light REE. However, the Lahroud patterns resemble REE patterns of pillow and basalt samples from the Mashhad ophiolite of northeastern Iran (Shafaii Moghadam et al., 2015a). All the patterns show strong LREE enrichment ($(\text{LaN}/\text{SmN})_{\text{ave}} = 3.47$). The REE patterns, together with clear similarities in the REE and Eu anomalies, suggest that these rocks are cogenetic and were derived from the same parental melt. The REE patterns of the metagabbro and granite are shown in Fig. 5e. These patterns are parallel to those of the basalts and gabbro, with nearly identical LREE enrichment ($(\text{LaN}/\text{SmN})_{\text{ave}} = 1.59$) and the same Eu pattern ($(\text{Eu}/\text{Eu}^*)_{\text{ave}} = 0.81$). However, the overall REE concentrations are higher, between 100 and 150_{chondrite}.

Isotope geochemistry. Three types of isotopic reservoirs are recognized in continental crust by Taylor et al. (1984), which were characterized in relation to Nd, Sr, and Pb isotopes. Zindler and Hart (1986) detected five members in the compositions of mantle, which is confirmed by all observations on midocean-ridge and oceanic-island basalts with a diversity of the mixing process. The contents of the mantle sources are summarized in Table 4 and plotted as a series of generalized isotopic correlation diagrams (Fig. 6). Isotope data on pillow lavas and gabbro samples are summarized in Fig. 6 and Table 4.

Based on Table 4, the Pb, Sr, and Nd contents of the Lahroud samples show BSE to HIMU composition. Data for the Lahroud sample variation of the isotope ratio of Nd to Pb plot near EM2 and EM1 and indicate an enriched mantle source (adapted from (Hart, 1986)). The data for the Lahroud samples plot the data source in variation of the isotope ratio of Nd to Sr and plot as the Bulk Silicate Earth (BSE) (Zindler and Hart, 1986). This composition is equivalent to a homogenous primitive mantle that formed by degassing of the planet. Some oceanic basalt has an isotope composition closely linked to the compositions of the bulk Earth to the present (Rollinson, 1993). Generally, the enrichment is likely to be related to a subduction environment; thereby crustal materials were subducted into the mantle via subduction erosion or in a related process. EMII has an affinity of the upper continental crust, which might represent a recycling of continentally raised sediments, continental crust, deformed ocean crust, or oceanic-island crusts. Then it is suggested that the enrichment is related to the mixing of the subcontinental lithosphere with the mantle. EMI with an affinity related to the lower crust probably represents a recycling process with lower crustal materials and suggests enrichment by the mantle metasomatism process. Weaver (1991) suggested that EMI and EMII are produced by mixing of HIMU mantle and subduction oceanic sediments (Rollinson, 1993; Plank and Langmuir, 1998).

In Fig. 6c, the data for the Lahroud samples variation of the isotope ratios of $^{207}\text{Pb}/^{204}\text{Pb}$ and $^{206}\text{Pb}/^{204}\text{Pb}$ plot near EM2 and indicate an enriched mantle source (adapted from (Hart, 1986)). Enriched mantle has variable $^{87}\text{Sr}/^{86}\text{Sr}$, low $^{143}\text{Nd}/^{144}\text{Nd}$ with high $^{207}\text{Pb}/^{204}\text{Pb}$, and $^{208}\text{Pb}/^{204}\text{Pb}$ with given values of $^{206}\text{Pb}/^{204}\text{Pb}$. Zindler and Hart (1986) differentiate between enriched mantle types II (EMII) with high $^{87}\text{Sr}/^{86}\text{Sr}$ (Fig. 6a, b). Because of similarities between these areas and Mashhad ophiolite, we plotted our isotope data with them for comparison. According to Fig. 6c–f, the Lahroud data plot as Pacific–Atlantic MORB and Indian MORB. At the same time, based on Fig. 6d–f, the data show characteristics of Pacific–Atlantic MORB and Indian MORB with subducted sediments. Shafaii Moghadam et al. (2015a) presented evidence that the Mashhad ophiolites have high and variable $^{207}\text{Pb}/^{204}\text{Pb}$, $^{208}\text{Pb}/^{204}\text{Pb}$, and $^{87}\text{Sr}/^{86}\text{Sr}$ in igneous rocks, which indicates alteration and reflection of the rocks with seawater and/or pollution by continental crusts and (or) the presence of subducted terrigenous sedimentary materials in the source.

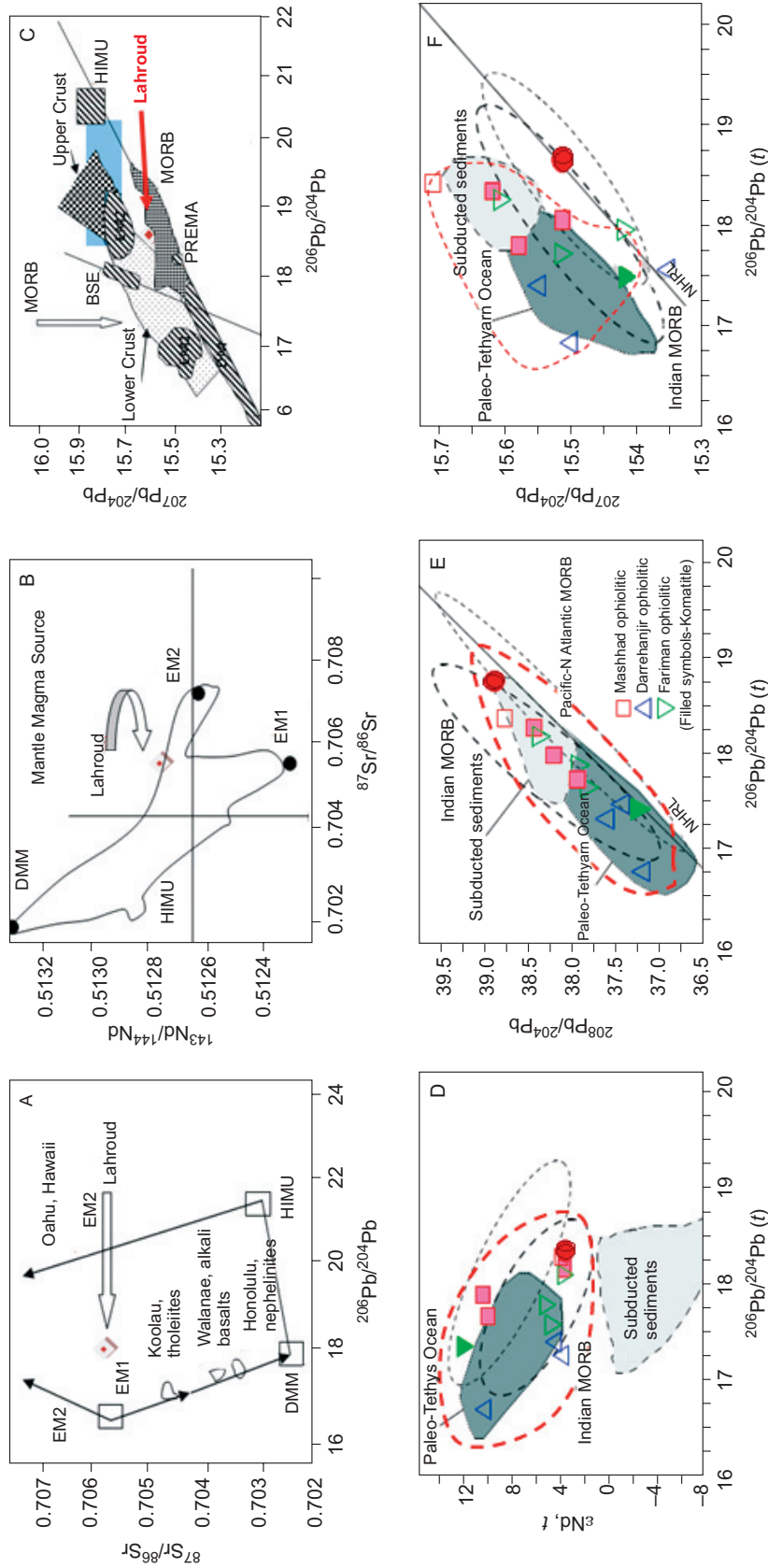


Fig. 6. Variation of the Sr and Pb isotope ratio of the Lahroud basalts (a), adapted from (Hart, 1986); Hawaiian data from (Stille et al., 1983); b, variation of the Nd and Sr isotope ratio of the Lahroud basalt, adapted from (Hart, 1986); c, $^{206}\text{Pb}/^{204}\text{Pb}$ vs. $^{207}\text{Pb}/^{204}\text{Pb}$ isotope correlation diagram for separation of source.

DM, Depleted mantle; BSE, bulk Earth silicate; EM1, EM2, enriched mantle; HIMU, mantle with high U/Pb; PREMA, with high mantle composition. The Lahroud sample is located very close to EM1 with ocean pelagic sedimentary rocks. d, ϵNd vs. $^{206}\text{Pb}/^{204}\text{Pb}$; e, $^{208}\text{Pb}/^{204}\text{Pb}$ vs. $^{206}\text{Pb}/^{204}\text{Pb}$; f, $^{207}\text{Pb}/^{204}\text{Pb}$ vs. $^{206}\text{Pb}/^{204}\text{Pb}$. Red dashed line shows the isotopic variation ranges in the Mashhad sample, and red circles show data from Lahroud.

⁴⁰Ar/³⁹Ar DATING

Despite the intense weathering and alteration process in this old area, the dated selected samples from a large number of rocks showed good results (some of the selected minerals in the samples did not yield suitable and reliable results). This ⁴⁰Ar/³⁹Ar incremental heating ages report is the first information on the cooling ages

of the oceanic crust in the Lahroud ophiolite. We present all ⁴⁰Ar/³⁹Ar experimental results in Tables 3 and 6 and Fig. 7. In two samples, good plateaus are apparent, indicating accurate ages of 347.0 ± 4.9 Ma and 187.7 ± 7.7 Ma for the amphibolite metamorphic unit and pillow lava, respectively.

Two samples from mineral concentrate (40–50 grains) were prepared from representative specimens of pillow lava basaltic rock and amphibolite in Lahroud, following crushing, washing, and handpicking under the binocular microscope. Glass concentrates from sample Oph7, representing the Lahroud pillow lava cooling age, and muscovite concentrates from sample Oph15, also from the amphibolite metamorphic unit, which represents metamorphic age, were provided.

Sample Oph7 produced a plateau age, and the isochron age revealed initial compositions near the atmospheric value to confirm a reliable total fusion age of 187.7 ± 7.7 Ma. The isochron age (190.3 ± 6.5 Ma) is concordant but has a slightly larger fit uncertainty than plateau age (Fig. 7b). The Lahroud ophiolite was mostly coeval with the Mashhad and other Paleo-Tethys ophiolites in a W–E suture zone. However, for sample Oph15, which produced a plateau age, the isochron revealed an initial composition like the atmospheric values

Table 6. ⁴⁰Ar/³⁹Ar measurements of muscovite separate in amphibolite from the Lahroud ophiolite complex

Sample	Mineral	Normal isochron	Inverse isochron	⁴⁰ Ar/ ³⁹ Ar Plateau age
Oph15	Muscovite	343.0 ± 13.0 Ma	344 ± 18 Ma	347.0 ± 4.9 Ma
Oph7	Glass	187.7 ± 7.7 Ma	190.3 ± 6.5 Ma	177.9 ± 3.9 Ma

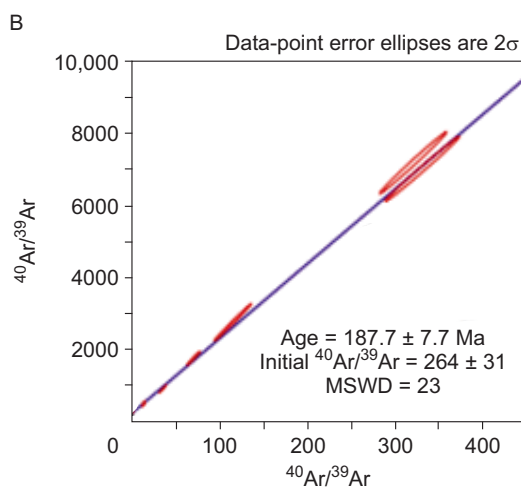
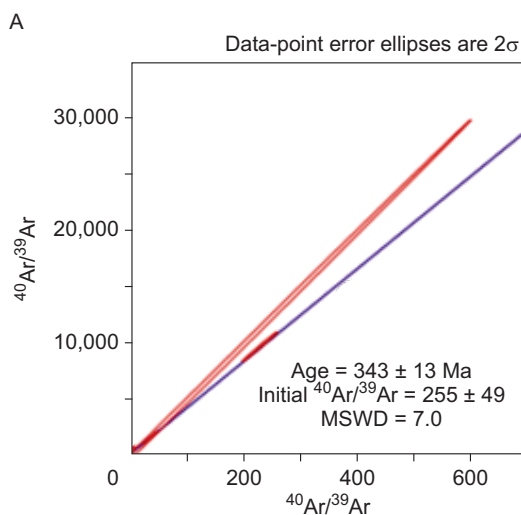
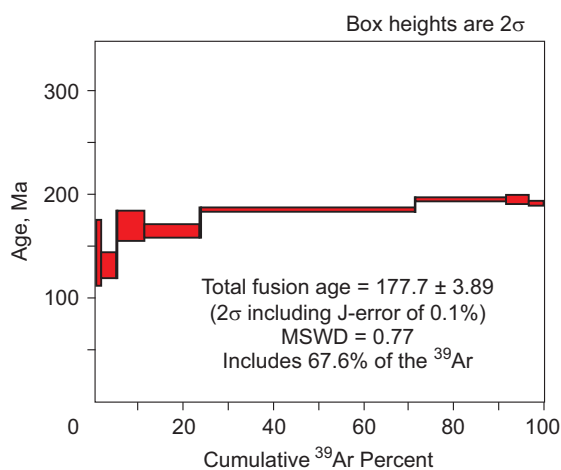
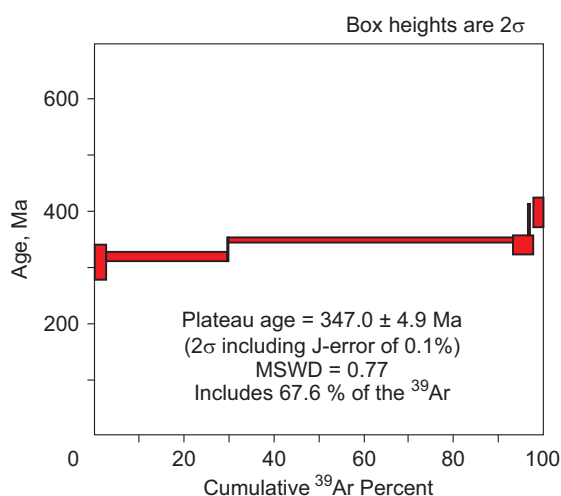


Fig. 7. ⁴⁰Ar/³⁹Ar age spectra for muscovite (amphibolite) and glass (basalt) separated from the Lahroud ophiolite sequence.

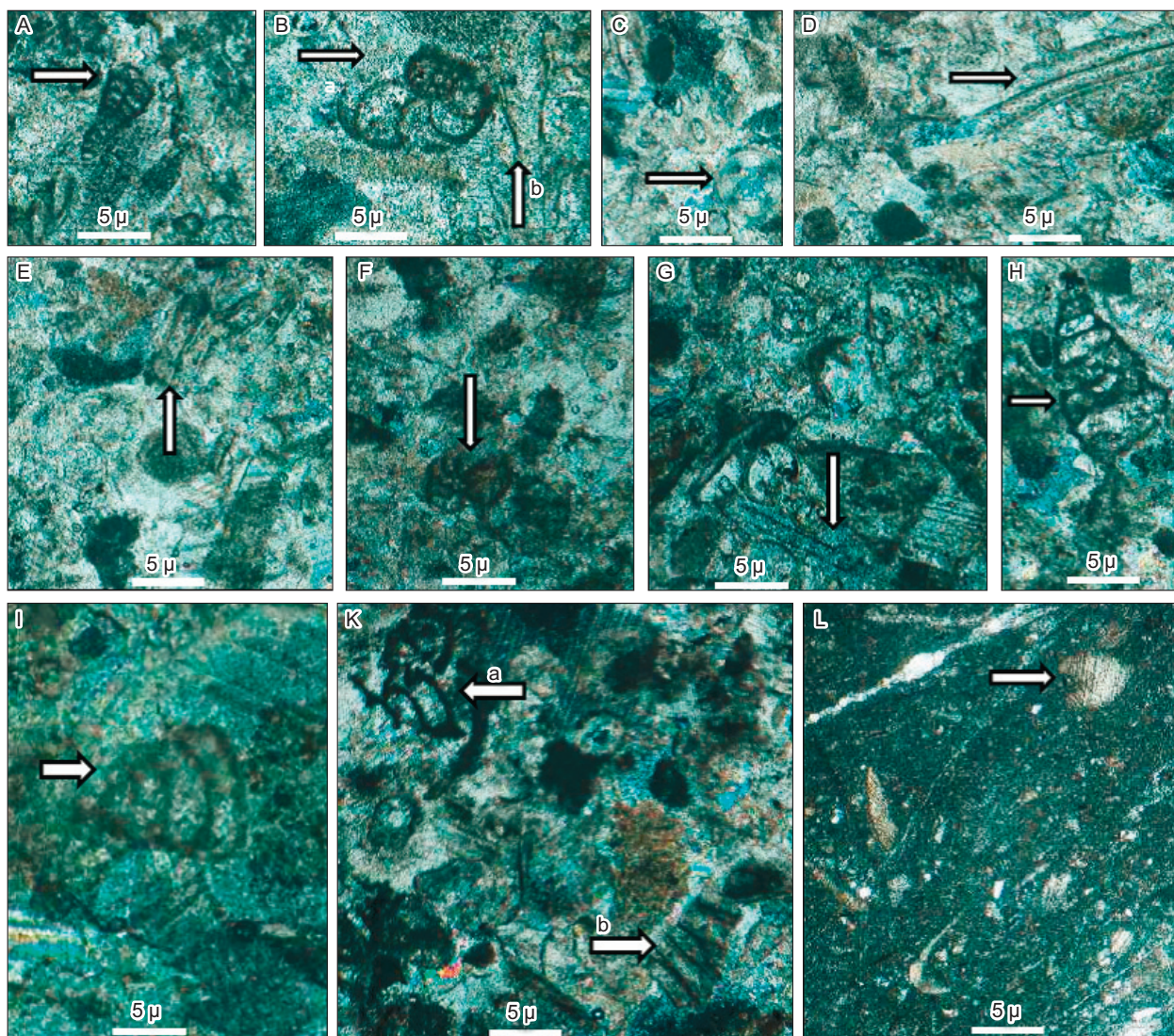


Fig. 8. Thin sections photographs with micropaleontological finds.

A, *Palaeotextularia* sp. (Upper Pennsylvanian, Carboniferous); B, a, *Nodosinella* cf. *concinna* Brady (Upper Mississippian?, Carboniferous); b, *Pseudokahlerina* sp. (Upper Carboniferous–lower Permian); C, *Nodosinella* cf. *cylindrica* (Brady) (Upper Mississippian? to Lower Pennsylvanian, Carboniferous); D, *Earlandia* sp. (Pennsylvanian, Carboniferous); E, *Earlandia* sp. (Pennsylvanian, Carboniferous); F, *Nodosinella* cf. *concinna* Brady (Upper Mississippian?, Carboniferous); G, *Endostaffella* sp. (Artinskian to Kungurian, Permian); H, *Laxoendothyra* sp. (Tournaisian to Visean, Carboniferous); I, *Pachyphloia* sp. (Pennsylvanian, Carboniferous); K, a, a piece of *Fusulinella* (*Staffella*) sp. (Artinskian to Kungurian, Permian); b, *Uralodiscus* sp. (Visean, Carboniferous); L *Bituberitina* sp. (Mississippian?, Carboniferous). The taxa considered in the present figures and Table 7 are referenced in (Loeblich and Tappan, 1988).

and confirmed a reliable plateau age (347 ± 4.9 Ma). The isochron age (343 ± 13 Ma) is concordant with it but has a slightly larger fit uncertainty than plateau age (347 ± 4.9 Ma) (Fig. 7a).

BIOSTRATIGRAPHIC STUDIES

Thirteen pelagic samples from sedimentary units in the Lahroud ophiolite were provided for micropaleontological study. Studies of thin sections of productive samples are illustrated in Fig. 8a–m and summarized in Table 7. Eftekharneshad and Behroozi (1991) indicated the early Permian biostratigraphic age for radiolarite intercalations with turbiditic units and lavas through the internal Iranian Paleo-Tethys suture zone with time. However, Zanchetta et al. (2013) indicated the late to early Permian and middle Permian time (~ 290 – 260 Ma). This is in accordance with the $^{40}\text{Ar}/^{39}\text{Ar}$ dating of hornblende gabbro from the Mashhad ophiolite with an age of 288 to 282 Ma (Ghazi et al., 2001) and the zircon U–Pb ages of 262.3 ± 1 Ma for the Anarak plagiogranite

Table 7. List of fossils found in pelagic limestone and cherts from the Lahroud ophiolite sequence in NW Iran

Samples	Fossils	Age	Fossil Reference
Oph2*	<i>Nodosinella cf. concinna</i> (Brady)	Upper Mississippian?, Carboniferous	(Brady, 1876)
Oph3*	<i>Nodosinella cf. cylindrica</i> (Brady)	Upper Mississippian? to lower Pennsylvanian, Carboniferous	(Brady, 1876)
Oph6*	<i>Endothyra baileyi</i> (Hall)	Mississippian?, Carboniferous	(Hall, 1858)
Oph7*	<i>Endostaffella</i> sp. (Rozovskaya)	Lower Permian to middle Permian	(Rozovskaya, 1961)
Oph11*	<i>Staffella molleri</i> (Ozawa)	Pennsylvanian, Carboniferous	(Ozawa, 1925)
Oph12*	<i>Bituberitina bicamerata</i> (Miklukho-Maklay)	Mississippian?, Carboniferous, central Asia	(Miklukho-Maklay, 1965)
Oph13*	<i>Palaeotextularia grahamensis</i> (Cushman and Waters)	Upper Pennsylvanian, Carboniferous	(Cushman and Waters, 1927)

*All the fossils were studied by S. Senemari.

(Paleozoic ophiolites outcrop on the CIM) and 382–380 Ma for the Mashhad ophiolites Darrehanjir (Shafaii Moghadam et al., 2015a).

DISCUSSION

This research deals with (1) age constraint to understand petrogenesis, (2) comparison to other Paleozoic ophiolites in Asia, and (3) tectonic settings. The ~160 Ma difference between the Carboniferous radiometric age of metamorphosed rocks and the Carboniferous (Mississippian? to Pennsylvanian) biostratigraphy of other rock units of the Lahroud mafic–ultramafic complex suggests that this is a part of the ophiolite complex that formed in the Carboniferous.

Petrogenesis and tectonic implications. By way of comparison, we plotted data on other Paleozoic ophiolites in Iran vs. the Lahroud volcanic and igneous rocks which show MORB characteristics with calc-alkaline affinity in this research. Trace element ratios are illustrated in Table 3 and Fig. 9, for comparing the Lahroud

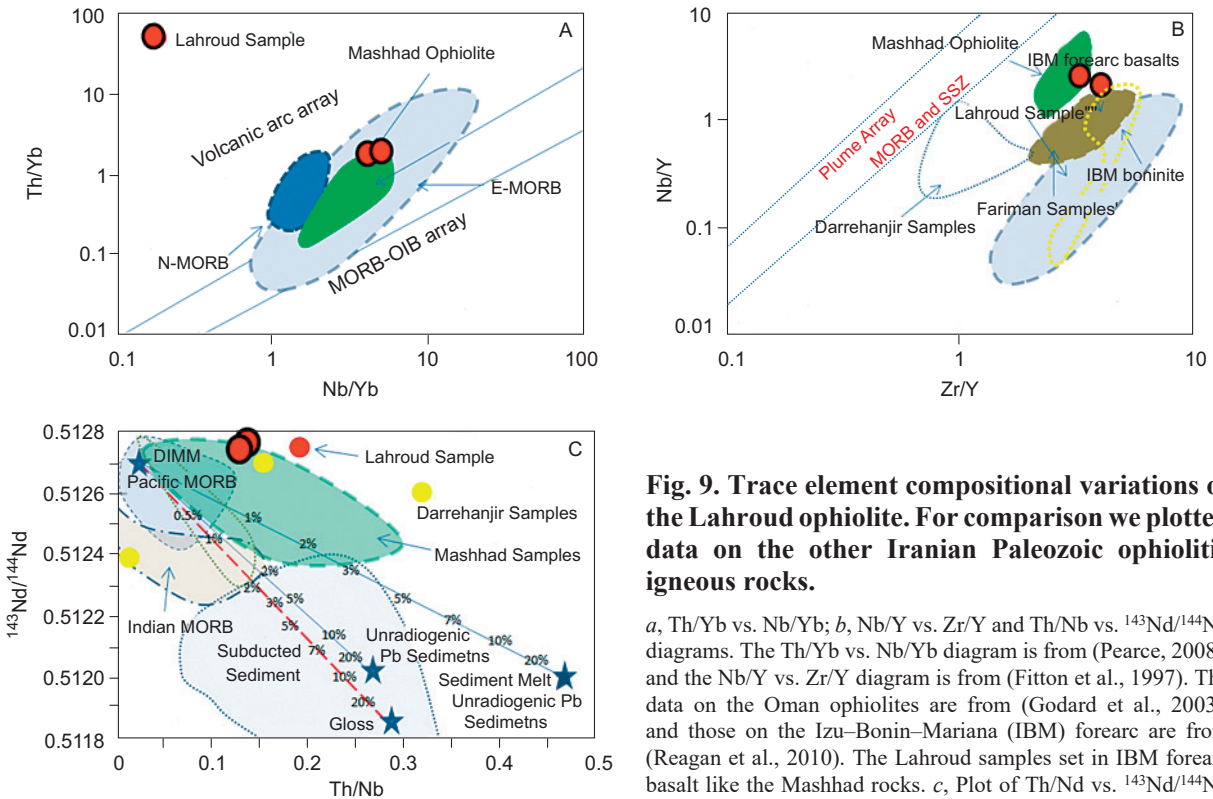


Fig. 9. Trace element compositional variations of the Lahroud ophiolite. For comparison we plotted data on the other Iranian Paleozoic ophiolitic igneous rocks.

a, Th/Yb vs. Nb/Yb; b, Nb/Y vs. Zr/Y and Th/Nb vs. $^{143}\text{Nd}/^{144}\text{Nd}$ diagrams. The Th/Yb vs. Nb/Yb diagram is from (Pearce, 2008), and the Nb/Y vs. Zr/Y diagram is from (Fitton et al., 1997). The data on the Oman ophiolites are from (Godard et al., 2003), and those on the Izu–Bonin–Mariana (IBM) forearc are from (Reagan et al., 2010). The Lahroud samples set in IBM forearc basalt like the Mashhad rocks. c, Plot of Th/Nd vs. $^{143}\text{Nd}/^{144}\text{Nd}$ for the Lahroud rock and other similar samples from the Paleo-

Tethys suture zone. The Darrehanjir–Mashhad igneous rocks are dispersed in this diagram, but in a binary array between the mantle wedge and sediment components. The mantle wedge end-member is very depleted Indian MORB mantle (DIMM) (Stracke et al., 2003) with high $^{143}\text{Nd}/^{144}\text{Nd}$ but low Th/Nd ratios, modified after (Liu et al., 2013; Shafaii Moghadam et al., 2015a).

rocks with the northeastern ophiolite rocks in Iran. Shafaii Moghadam et al. (2015a) showed that most rocks of Darrehanjir have high ratios of Th/Yb in contrast to Nb/Yb and showed higher values than mantle arrays, which indicates additional melt/fluids ratios from subduction-related sediment or continental-crust pollutions. The Th/Yb ratios in the Permian Fariman lavas, which plotted within enriched MORB mantle arrays, suggested a few enrichments from mantle sources and minor subduction-related influences, similar to those produced by mantle plumes (Shafaii Moghadam et al., 2015a) (Fig. 9a). The igneous rocks in Mashhad plotted between the Darrehanjir (high Th/Nb) and Fariman (low Th/Nb) rocks, and the values shown by the Lahroud rocks are close to the ranges shown by the Mashhad rocks. They compared igneous rocks from the Mashhad ophiolites with the Rasht, Jandagh–Anarak, and Aghdarband ophiolites, which appeared in relation to subduction features; thereby our data are very close to the data on the Mashhad rocks on the Nb/Y vs. Zr/Y ratio diagram (Fig. 9b).

Based on (Faure and Mensing, 2004), Nd is mostly immobile in fluid environments unless the water/rock ratio reaches $>10^5$ in the alteration process. Therefore, the $^{143}\text{Nd}/^{144}\text{Nd}$ in the studied rocks might be not influenced by seawaters via alteration. The mobility of U and Pb via hydrothermal alteration influenced Pb isotope contents in the affected rocks (Faure and Mensing, 2004). Additions of U by alteration can increase $^{206}\text{Pb}/^{204}\text{Pb}$ during the time. Because of the immobility of Th in the alteration process and the low abundances of ^{235}U , $^{207}\text{Pb}/^{204}\text{Pb}$, and $^{208}\text{Pb}/^{204}\text{Pb}$, these ratios in igneous rocks will reflect mantle sources (Liu et al., 2013). In detecting the contributions of sediment melts to a depleted mantle source in the Darrehanjir–Mashhad igneous rocks, Shafaii Moghadam et al. (2015a) used the diagram of $^{143}\text{Nd}/^{144}\text{Nd}$ vs. Th/Nd which was constructed by Liu et al. (2013) (Fig. 9c). Because of the immobility of Nd and Th in a fluid that is released from subduction-related oceanic crust and with related sediment, whereas they are mobile in the resource melt (Liu et al., 2013). According to Shafaii Moghadam et al. (2015b), the samples show a linear trend in mantle wedges (depleted Indian MORB mantle) and sediments (with a lower content of radiogenic Pb in the Izu–Bonin sediment (Plank et al., 2007)), and the Lahroud sample illustrates a behavior similar to that of the Mashhad samples (Fig. 9c). The Mashhad and Fariman komatiites show high $^{143}\text{Nd}/^{144}\text{Nd}$, which suggests a highly depleted mantle source lacking in any subducted sediments. The Darrehanjir–Mashhad complex of Devonian–Permian rocks that belonged to the Paleo-Tethys belt represented another Paleozoic oceanic basin that might be related to the CAO (Central Asian Orogenic Belt) (Shafaii Moghadam et al., 2015a).

Other Paleozoic ophiolites in Asia. The Tauric (Caucasus)–Küre (Turkey) mélange with some exotic block of Carboniferous–Permian pelagic limestones (Şengör, 1998; Zonenshain et al., 1990) suggests that the Paleo-Tethys extended as far west as Turkey. The Trans-Caucasian massif, which is situated among the Greater Caucasus in the north and the Lesser Caucasus in the south (Zakariadze et al., 2007), contained some evidence of early Paleozoic metamorphosed ophiolite units with sheeted dikes and pillow lava (Gamkrelidze et al., 1999; Rolland et al., 2011). A tectonized mélange zone in the north of the Sevan–Akera suture zone includes allochthonous pieces from middle Paleozoic rocks and was affected by early Variscan metamorphosed rocks, according to Ar–Ar dates (about 336 to 330 Ma) (Zakariadze et al., 2007; Treloar et al., 2009). Other remnants of the Paleo-Tethys are located in Turkmenistan (Boulin, 1988), which are interpreted as early Paleozoic to Late Devonian deep ocean sedimentary rocks and ophiolite; in the Kizilkaya and Tuar areas of Turkmenistan (Mir-sakhanov, 1989); early Paleozoic–Late Devonian rocks in Afghanistan, including flysch-type ones, belonging to the Cambrian and Ordovician to Silurian periods (Boulin, 1988); in the northeastern part of Afghanistan (in the western part of Hindu Kush and in the Badakhshan area (Boulin, 1988)); and on the Tibetan plateaus, which preserved remnants of the Paleo-Tethys Ocean and the following mixtures of the Laurasia and Gondwana supercontinents from the Paleozoic (Şengör and Natal'in, 1996; Zhai et al., 2013). Farther east, there is pillow lava from the north–northeast of Tajikistan (pelagic limestone intercalation with Famennian–Tournaisian rocks (~360 Ma)). The late Carboniferous and early Permian intrusions with volcanism in the Mediterranean and Caucasus areas are related to the northward subduction trend of the Paleo-Tethys beneath Eurasia (Stampfli and Borel, 2002; Rolland et al., 2011). Low-pressure and high-temperature metamorphic units outcrop in the south of Georgia, where Ar–Ar ages are about 303 Ma (Carboniferous time from (Rolland et al., 2011)). High-pressure rocks in the north of Iran (e.g., Shanderman in the Rasht ophiolite (Omrani et al., 2013)) with an Ar–Ar age of 330 Ma (Zanchetta et al., 2009) are inferred as Paleo-Tethys subduction channel ways. The southward trend of subduction beneath the north of the Tianshan arc (within the CAO, southeast of Kazakhstan) is probably responsible for the generation of 343 Ma SSZ-type plagiogranites and E-MORB with OIB-like gabbro with an age of 302 Ma (Li et al., 2014). The Carboniferous Kunlun arc, located in the north of the Pamir Mountains and northwest of Tibet through to magmatism in Tajikistan, is related to northward-vergent subduction settings (Schwab et al., 2004).

The Iran Paleo-Tethys suture zone. The Paleo-Tethys opened in the Early Ordovician (Stampfli et al., 1991), and subduction was initiated at 380 Ma at the southern edge of Eurasia and was probably diachronous as the Caucasus and Turkmenistan ophiolite, which represents the Carboniferous SSZ-type ocean crust. Zanchetta et al. (2013) concluded that the Paleozoic volcanosedimentary units in the Fariman–Darrehanjir areas

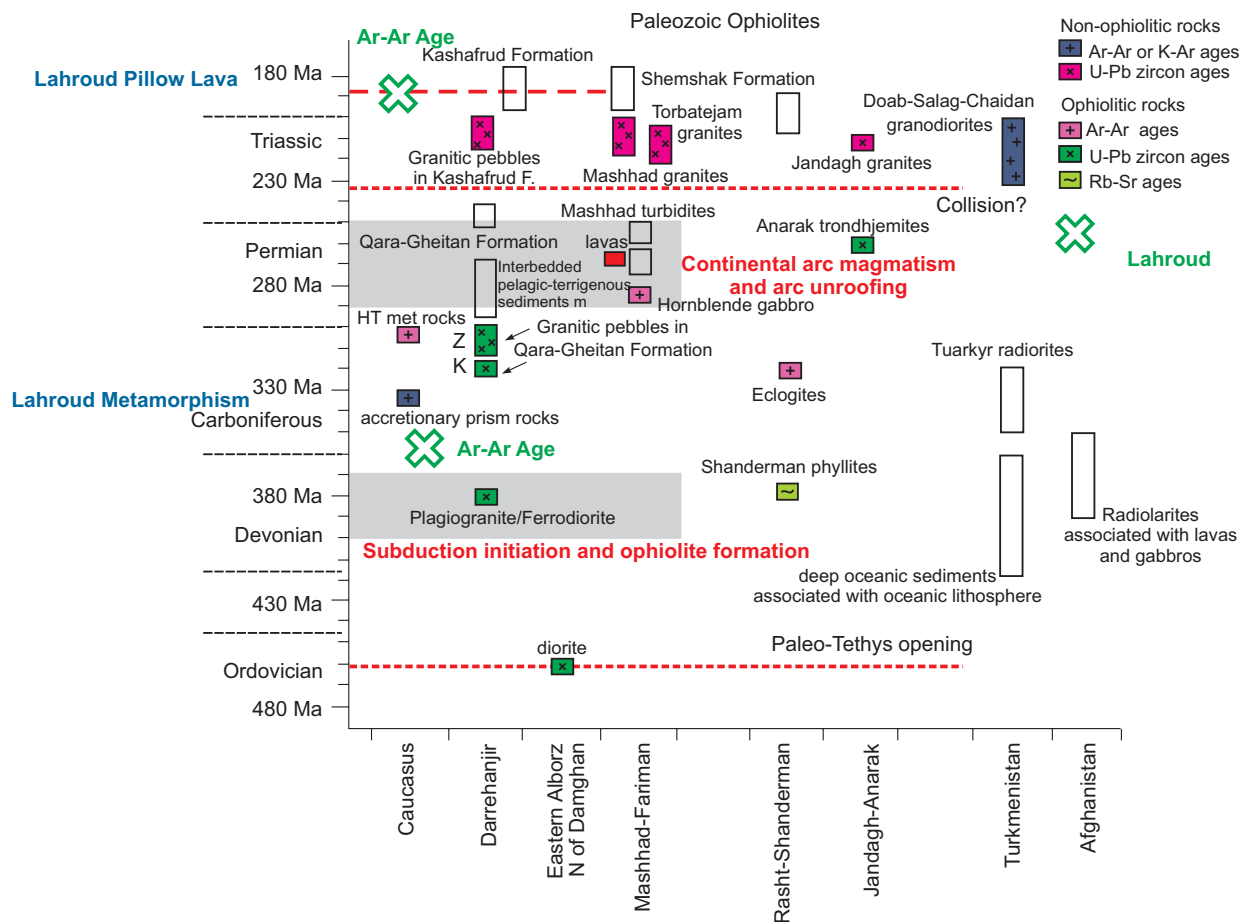


Fig. 10. Simplified chart showing the ages of igneous and sedimentary sequences that constrain the ages of the Iranian Paleozoic ophiolites; greenish area inside dashed lines encompasses ophiolite ages.

The U–Pb dating of granitic pebble from the Qara-Gheitan Formation (K) is from (Karimpour et al., 2010); the Ar–Ar age data on the Mashhad ophiolites, from (Ghazi et al., 2001); the U–Pb zircon ages of the Mashhad granites, from (Karimpour et al., 2010; Mirnejad et al., 2013); the Ar–Ar ages of the Rasht–Shanderman eclogites, from the U–Pb zircon age data on the Anarak trondhjemitites and Jandagh granites, from (Bagheri and Stampfli, 2008); the U–Pb zircon data on the Torbat-e-Jam granites, granitic pebble from the Qara-Gheitan Formation (Z), and granitic pebbles from the Kashafrud Formation, from (Zanchetta et al., 2013). The Ar–Ar ages of the Caucasus accretionary prism and high-*T* metamorphic rocks are from (Rolland et al., 2011); the data on the Turkmenistan and Afghanistan pelagic sediments are from (Garzanti and Gaetani, 2002; Zakariadze et al., 2007; Treloar et al., 2009) and (Boulin, 1988), respectively, at 347–187 Ma, modified after (Shafaii Moghadam et al., 2015a).

are Permian. They also conclude that the Fariman–Darrehanjir igneous rocks developed as remnants of a magmatic arc on the south margin of Eurasia, in the upper part of the northward-dipping Paleo-Tethys subduction zone, which was an active margin from the Carboniferous. According to (Shafaii Moghadam et al., 2015a), U–Pb age data, geochemistry, and occurrences of abyssal peridotites in association with Devonian boninite to calc-alkaline gabbro/plagiogranites support their U–Pb age data and demonstrate a pulse of SSZ-type ocean crust forming in the Early to Late Devonian (Fig. 10). Permian igneous rocks in association with terrigenous/pelagic sedimentary rocks might represent magmatism and sediments in the subduction-related setting at the foot of the Eurasian margin, similar to the accretionary orogeny with fragments, in Devonian ocean crust and then followed by Permian igneous rocks. Geochronology data on granite–granodiorite intrusions into the Mashhad and Torbat-e-Jam ophiolites yielded U–Pb ages of 215 ± 4 and 217 ± 4 Ma (Karimpour et al., 2010) and 199.8 ± 3.7 and 217 ± 4 Ma (Mirnejad et al., 2013; Zanchetta et al., 2013). Northward subduction of the Paleo-Tethys oceanic lithosphere zone started at the southern margin of Eurasia in the middle–Later Paleozoic (Alavi, 1991; Metcalfe, 2006; Zanchi et al., 2009) (Fig. 10) in Iran, Afghanistan, the Caucasus, and Turkey. The Lahroud is therefore inferred to represent a part of the Paleo-Tethys suture zone in the northwestern part of Iran, with a metamorphic event at 347 Ma as a part of metamorphic regime in a thickened oceanic crust (Fig. 7a) affected by subduction processing. Dating from pillow lava (basalts) gives an age for the closure of the ophiolitic system in the region (Fig. 7b).

CONCLUSIONS

(1) The Lahroud Ophiolite is, apparently, an ophiolitic complex in association with a basal metamorphic “zone” in the Paleo-Tethys oceans; (2) the Lahroud Ophiolite comprises a typical sequence of ophiolitic rocks; (3) the volcanic rocks represent the upper part of the ophiolite rock in the region, overlain by fossiliferous pelagic limestones and radiolarian cherts. Radiometric dating on amphibolite and basalt (pillow lava) clearly suggests the end of the Paleozoic (Carboniferous) as a maximum age for the beginning of formation of the ophiolitic complex. The chronostratigraphy data that resulted from pelagic limestone biostratigraphy studies yield the same age. These ages are (late Paleozoic) Mississippian? to Pennsylvanian. Younger age for pillow lava indicates the continuation of formation of “Lahroud oceanic crust” in the late Carboniferous to Early Jurassic. Consequently, it is inferred that the Lahroud Ophiolite formed as a result of the closure of this part of the Paleo-Tethys. We propose that the subduction and closing of the oceanic crust started almost at 340 Ma, and we see strong metamorphism as a fingerprint in the region. The scenario continued until 180 Ma and ended with the formation of basaltic pillow lava volcanic extrusive rocks. The results show that the Lahroud “ophiolite” is an igneous complex; biostratigraphy and Ar–Ar age studies in the area indicate Permian age, but the Ar–Ar ages of pillow lavas indicate Early Jurassic (Pliensbachian) crystallization and early Carboniferous (Tournaisian) for metamorphosed units. This is another piece in the jigsaw of the Paleo-Tethys in northwestern Iran and its continuation to the Mashhad–Rasht suture zone. This research has obtained additional constraints on the configuration of the Paleo-Tethys in the Devonian to Early Jurassic in Iran, especially in the Lahroud region.

The author thanks Dr. Weis from the Noble Gas Laboratory, Pacific Centre for Isotopic and Geochemical Research, University of British Columbia (Vancouver), for dating and isotopic data, and Dr. Saeedeh Senemari for study of fossils in the biostratigraphy section. The author is grateful to Andrew Tunningly and Dr. David Lentz, who kindly commented on the preliminary version of the manuscript. Special thanks go to Prof. Wolf-Christian F.A. Dullo and Dr. Albrecht von Quadt for their useful suggestions, remarks, and recommendations in finalizing the manuscript.

REFERENCES

- Aftabi, A., Fathi, G.,** 1992. Geology and mining potential of the ophiolitic belt of Kamroud and Shahr-e-Babak [in Persian]. *Min. Metals* 50, 60–74.
- Aharipour, R., Moussavi, M.R., Mosaddegh, H., Mistiaen, B.,** 2010. Facies features and paleoenvironmental reconstruction of the Early to Middle Devonian syn-rift volcano-sedimentary succession (Padeha Formation) in the Eastern-Alborz Mountains, NE Iran. *Facies* 56, 279–294.
- Alavi, M.,** 1991. Sedimentary and structural characteristics of the Paleo-Tethys remnants in northeastern Iran. *GSA Bull.* 103, 983–992.
- Alavi, M.,** 1992. Thrust tectonics of the Binaload region, NE Iran. *Tectonics* 11, 360–370.
- Alavi, M.,** 1996. Tectonostratigraphic synthesis and structural style of the Alborz Mountain system in northern Iran. *J. Geodyn.* 21, 1–33.
- Amidi, M., Babakhani, A.R., Nazer, N.H.,** 1991. Lahroud map. *Geol. Surv. Iran.*
- Anonymous,** 1972. Penrose field conference on ophiolites. *Geotimes* 17 (12), 22–24.
- Arvin, M., Robinson, P.T.,** 1994. The petrogenesis and tectonic setting of lavas from the Baft ophiolitic melange, southwest of Kerman, Iran. *Can. J. Earth Sci.* 31, 824–834.
- Bagheri, S., Stampfli, G.M.,** 2008. The Anarak, Jandaq and Posht-e-Badam metamorphic complexes in central Iran: New geological data, relationships and tectonic implications. *Tectonophysics* 451, 123–155.
- Berberian, M., Amidi, S.M., Babakhani, A.,** 1981. Discovery of the Qaradagh ophiolite belt, the southern continuation of the Sevan-Akera (Little Caucasus) ophiolite belt in northwestern Iran (Ahar quadrangle); a preliminary field note. *Geol. Surv. Iran, Internal Rep* [in Persian].
- Boulin, J.,** 1988. Hercynian and Eocimmerian events in Afghanistan and adjoining regions. *Tectonophysics* 148, 253–278.
- Brady, H.B.,** 1876. A monograph of the Carboniferous and Permian foraminifera (the genus *Fusulina* excepted). *Palaeontogr. Soc., London.*
- Campbell, K., Ghazi, A.M., LaTour, T., Hassanipak, A.A.,** 2000. Geochemistry, petrology and tectonics of the Shahr-e-Babak ophiolite, SE Iran. *Abstracts with Programs, GSA, Southeastern Sect.* 31, 9.
- Cushman, J.A., Waters, J.A.,** 1927. Arenaceous Paleozoic Foraminifera from Texas. *Contributions from the Cushman Laboratory for Foraminiferal Research, Vol. 3, Part 3,* 146–155.
- Delaloye, M., Desmons, J.,** 1980. Ophiolites and melange terranes in Iran: a geochronological study and its paleotectonic implications. *Tectonophysics* 68, 83–111.
- Desmons, J., Beccaluva, L.,** 1983. Mid-oceanic ridge and island arc affinities in ophiolites from Iran: paleogeographic implication. *Chem. Geol.* 39, 39–63.
- Dilek, Y.,** 2003. Ophiolite concept and its evolution, in: Dilek, Y., Newcomb, S. (Eds.), *Ophiolite Concept and the Evolution of Geological Thought.* *GSA Spec. Pap.* 373, 1–16.

- Eftekharneshad, J., Behroozi, A.**, 1991. Geodynamic significance of recent discoveries of ophiolites and Late Paleozoic rocks in NE Iran (including Kopet Dagh). *Abh. Geol. Bundesanst.* 38, 89–100.
- Faure, G., Mensing, T.**, 2004. *Isotopes: Principles and Applications*. Wiley.
- Fitton, J.G., Saunders, A.D., Norry, M.J., Hardason, B.S., Taylor, R.N.**, 1997. Thermal and chemical structure of the Iceland plume. *Earth Planet. Sci. Lett.* 153, 197–208.
- Gamkrelidze, I.P., Shengelia, D.M., Shvelidze, I.U., Vashakidze, G.T.**, 1999. The new data about geological structure of the Lokhi crystalline massif and Gorastskali metaophiolites. *Proc. Geol. Inst. Acad. Sci. Georgia, New Ser.* 114, 82–108.
- Garzanti, E., Gaetani, M.**, 2002. Unroofing history of late Paleozoic magmatic arcs within the “Turan plate” (Tuarkyr, Turkmenistan). *Sediment. Geol.* 151, 67–87.
- Ghazi, A.M., Hassanipak, A.A.**, 1999. Geochemistry and petrology of subalkaline and alkaline extrusives of Kermanshah ophiolite, Zagros Suture Zone, SW Iran. *J. Asian Earth Sci.* 17, 319–332.
- Ghazi, A.M., Hassanipak, A.A., Duncan, R.A., Hogan, L.G., Mahoney J.J.**, 1997a. Geochemistry, $^{40}\text{Ar}/^{39}\text{Ar}$ ages and preliminary isotopic analyses of the Khoy ophiolite, northwestern Iran. *EOS (Trans. AGU)* 79, F654.
- Ghazi, A.M., Hassanipak, A.A., Wallace, K.**, 1997b. Geochemistry, petrology and geology of the Sabzevar ophiolite, northeastern Iran: implication on Tethyan tectonics. *Abstracts with Programs, GSA*, 29, A-229.
- Ghazi, A.M., Chatham, B., Hassanipak, A.A., Mahoney, J.J., Duncan, R.A.**, 1999. A petrogenetic investigation of the Khoy ophiolite, NW Iran: implications for Tethyan magmatism and ophiolite genesis. *RIDGE Field School: The Troodos Ophiolite and Mid-Ocean Ridge Processes: Abstract and Field School Notes*, Larnaca, Cyprus, July 1999. Oregon State Univ., p. 13.
- Ghazi, M., Hassanipak, A.A., Tucker, P.J., Mobasher, K.**, 2001. Geochemistry and $^{40}\text{Ar}-^{39}\text{Ar}$ ages of the Mashhad Ophiolite, NE Iran. *EOS (Trans. AGU)* 82 (47), Fall Meeting.
- Ghazi, A.M., Pessagno, E.A., Hassanipak, A.A., Kariminia, S.M., Duncan, R.A., Babaie, H.A.**, 2003. Biostratigraphic zonation and $^{40}\text{Ar}-^{39}\text{Ar}$ ages for the Neotethyan Khoy ophiolite of NW Iran. *Palaeogeogr. Palaeoclimatol. Palaeoecol.* 193 (2), 311–323.
- Godard, M., Dautria, J.M., Perrin, M.**, 2003. Geochemical variability of the Oman ophiolite lavas: relationship with spatial distribution and paleomagnetic directions. *Geochem. Geophys. Geosyst. (G)* 4, 8609, doi: 10.1029/2002GC000452.
- Hall, J.**, 1858. Description of new species of fossils from the Carboniferous limestones of Indiana and Illinois. *Trans. Albany Inst.* 4, 1–36.
- Hart, S.R.**, 1986. A large-scale isotope anomaly in the Southern Hemisphere mantle. *Nature* 309, 753–757.
- Hassanipak, A.A., Ghazi, A.M.**, 2000. Petrology, geochemistry and tectonic setting of the Khoy ophiolite, Northwest Iran. *J. Asian Earth Sci.* 18, 109–121.
- Hassanipak, A.A., Ghazi, A.M., Wampler, J.M.**, 1996. REE characteristics and K/Ar ages of the Band-e-Zeyarat ophiolite complex, southeastern Iran. *Can. J. Earth Sci.* 33, 1534–1542.
- Hassanipak, A.A., Ghazi, A.M., Duncan, R.A., Pessagno, E.A., Kariminia, S.M., Mobasher, K.**, 2002. Spatial and temporal distribution of Paleo- and Neo-Tethys ophiolites in Iran and their tectonomagmatic significance. *Abstracts with Programs, GSA*, 37, 331.
- Irvine, T.N., Baragar, W.R.A.**, 1971. A guide to chemical classification of common volcanic rocks. *Can. J. Earth Sci.* 8, 523–547.
- Karimpour, M.H., Stern, C.R., Farmer, G.L.**, 2010. Zircon U–Pb geochronology, Sr–Nd isotope analyses, and petrogenetic study of the Dehnow diorite and Kuhsangi granodiorite (Paleo-Tethys), NE Iran. *J. Asian Earth Sci.* 37, 384–393.
- Lanphere, M.A., Pamić, J.**, 1983. $^{40}\text{Ar}/^{39}\text{Ar}$ ages and tectonic setting of ophiolite from the Neyriz area, southeast Zagros Range, Iran. *Tectonophysics* 96 (3), 245–256.
- Lensch, G.**, 1980. Major element geochemistry of the ophiolites in north-eastern Iran, in: Panayiotou, A. (Ed.), *Ophiolites: Proc. Int. Ophiolite Symp.*, Ministry of Agriculture and Natural Resources. Geol. Surv. Department, Republic of Cyprus, pp. 398–401.
- Lensch, G., Mihm, A., Alavi-Tehrani, N.**, 1977. Petrography and geology of the ophiolite belt north of Sabzevar/Khorasan (Iran). *Neues Jahrb. Mineral. Abh.* 131, 156–178.
- Li, C., Xiao, W., Han, C., Zhou, K., Zhang, J., Zhang, Z.**, 2014. Late Devonian–early Permian accretionary orogenesis along the North Tianshan in the southern Central Asian Orogenic Belt. *Int. Geol. Rev.* 57 (5–8), 1023–1050.
- Lippard, S.J., Shelton, A.W., Gass, I.G.**, 1986. The ophiolite of Northern Oman. *Mem. Geol. Soc. London* 11.
- Liu, X., Xu, J., Castillo, P.R., Xia, W., Shi, Y., Fenga, Z., Guo, L.**, 2013. The Dupal isotopic anomaly in the southern Paleo-Asian Ocean: Nd–Pb isotope evidence from ophiolites in Northwest China. *Lithos* 189, 185–200.

- Loeblich, A.R., Tappan, J.H.**, 1988. Foraminiferal Genera and Their Classification. Van Nostrand Reinhold, New York.
- McCall, G.J.H.**, 1985. Area report, east Iran, area no. 1. Geol. Surv. Iran Rep. 57.
- McCall, G.J.H.**, 1997. The geotectonic history of the Makran and adjacent areas of southern Iran. *J. Asian Earth Sci.* 15, 517–531.
- Meng, F., Cui, M., Wu, X., Ren, Y.**, 2013. Heishan mafic–ultramafic rocks in the Qimantag area of Eastern Kunlun, NW China: Remnants of an early Paleozoic incipient island arc. *Gondwana Res.* 23, 825–836.
- Meschede, M.**, 1986. A method of discriminating between different types of mid-ocean ridge basalts and continental tholeiites with the Nb-Zr-Y diagram. *Chem. Geol.* 56, 207–218.
- Metcalf, I.**, 2006. Paleozoic and Mesozoic tectonic evolution and palaeogeography of East Asian crustal fragments: The Korean Peninsula in context. *Gondwana Res.* 9 (1–2), 24–46.
- Miklukho-Maklay, A.D.**, 1965. Some Middle Paleozoic foraminifera from Central Asia. *Ezhegodnik Vses. Paleontologichesk. O–va.* 17, 30–40.
- Mirnejad, H., Lalonde, A.E., Obeid, M., Hassanzadeh, J.**, 2013. Geochemistry and petrogenesis of Mashhad granitoids: an insight into the geodynamic history of the Paleo-Tethys in northeast of Iran. *Lithos* 170–171, 105–116.
- Mirsakhanov, M.W.** (Ed.), 1989. Geologic Map of Turkmenistan, Scale 1:500,000 [in Russian]. *Turkmengeologiya*, Ashkhabad.
- Omran, H., Moazzen, M., Oberhansli, R., Tsujimori, T., Bousouet, R., Moayyed, M.**, 2013. Metamorphic history of glaucophane-paragonite-zoisite eclogites from the Shanderman area, northern Iran. *J. Metamorph. Geol.* 31, 91–812.
- Ozawa, Y.**, 1925. Palaeontological and stratigraphical studies on the Permo-Carboniferous limestone of Nagata, Part 2. *Palaeontology. J. Coll. Sci. Tokyo Imp. Univ.* 45 (6), 1–90.
- Pearce, J.A.**, 2008. Geochemical fingerprinting of oceanic basalts with applications to ophiolite classification and the search for Archean oceanic crust. *Lithos* 100, 14–48.
- Plank, T., Langmuir, C.H.**, 1998. The chemical composition of subducting sediment and its consequences for the crust and mantle. *Chem. Geol.* 145 (3–4), 325–394, doi: 10.1016/S0009-2541(97)00150-2.
- Plank, T., Kelley, K.A., Murray, R.W., Stern, L.Q.**, 2007. Chemical composition of sediments subducting at the Izu–Bonin trench. *Geochem. Geophys. Geosyst.* 8, doi: 10.1029/2006GC001444.
- Reagan, M.K., Ishizuka, O., Stern, R.J., Kelley, K.A., Ohara, Y., Blichert-Toft, J., Bloomer, S.H., Cash, J., Fryer, P., Hanan, B.B., Hickey-Vargas, R., Ishii, T., Kimura, J.I., Peate, D.W., Rowe, M.C., Woods, M.**, 2010. Fore-arc basalts and subduction initiation in the Izu-Bonin-Mariana system. *Geochem. Geophys. Geosyst.* 11, Q03X12, doi: 10.1029/2009GC002871.
- Renne, P.R., Swisher, C.C., Deino, A.L., Karner, D.B., Owens, T., DePaolo, D.J.**, 1998. Intercalibration of standards, absolute ages and uncertainties in $^{40}\text{Ar}/^{39}\text{Ar}$ dating. *Chem. Geol., Isot. Geosci. Sect.* 145 (1–2), 117–152.
- Rolland, Y., Sosson, M., Adamia, Sh., Sadradze, N.**, 2011. Prolonged Variscan to Alpine history of an active Eurasian margin (Georgia, Armenia) revealed by $^{40}\text{Ar}/^{39}\text{Ar}$ dating. *Gondwana Res.* 20 (4), 798–815.
- Rollinson, H.R.**, 1993. *Using Geochemical Data: Evaluation, Presentation, Interpretation.* Longman Scientific and Technical, London.
- Rozovskaya, S.E.**, 1961. On the systematics of the families Endothyridae and Ozawinellidae. *Paleontologicheskii Zhurnal.* No. 3, 19–21.
- Sarkarinejad, K.**, 1994. Petrology and tectonic setting of the Neyriz ophiolite, southeast Iran, in: Ishiwatari, A., Malpas, A., Ishizuka, H. (Eds.), *Circum-Pacific Ophiolites (Proc. 29th Int. Geol. Congr., Part D)*. VSP, Utrecht, pp. 221–234.
- Schwab, M., Ratschbacher, L., Siebel, W., McWilliams, M., Minaev, V., Lutkov, V., Chen, F., Stanek, K., Nelson, B., Frisch, W., Wooden, J.L.**, 2004. Assembly of the Pamirs: Age and origin of magmatic belts from the southern Tien Shan to the southern Pamirs and their relation to Tibet. *Tectonics* 23 (4), doi: 10.1029/2003TC001583.
- Şengör, A.M.C.**, 1998. Die Tethys: vor hundert Jahren und heute. *Mitt. Österr. Geol. Ges.* 89, 5–176.
- Şengör, A.M.C., Natal'in, B.A.**, 1996. Paleotectonics of Asia: Fragments of a synthesis, in: Yin, A., Harrison, T.M. (Eds.), *The Tectonic Evolution of Asia.* Cambridge Univ. Press, Cambridge, pp. 486–640.
- Shafaii Moghadam, H., Stern, R.J.**, 2011. Geodynamic evolution of upper Cretaceous Zagros ophiolites: formation of oceanic lithosphere above a nascent subduction zone. *Geol. Mag.* 148, 762–801.
- Shafaii Moghadam, H., Zaki Khedr, M., Arai, S., Stern, R.J., Ghorbani, G., Tamura, A., Ottley, C.J.**, 2015a. Arc-related harzburgite–dunite–chromitite complexes in the mantle section of the Sabzevar ophiolite, Iran: a model for formation of podiform chromitites. *Gondwana Res.* 27 (2), 575–593, doi: org/10.1016/j.gr.2013.09.007.

Shafai Moghadam, H., Li, X.H., Ling, X.X., Stern, R.J., Khedr, M.Z., Chiaradia, M., Ghorbani, G., Shoji, A., Tamura, A., 2015b. Devonian to Permian evolution of the Paleo-Tethys Ocean: New evidence from U–Pb zircon dating and Sr–Nd–Pb isotopes of the Darrehanjir-Mashhad “ophiolites”, NE Iran. *Gondwana Res.* 28 (2), 781–799.

Shi, R., Griffin, W.L., O'Reilly, S.Y., Huang, Q., Zhang, X., Liu, D., Zhi, X., Xia, Q., Ding, L., 2012. Melt/mantle mixing produces podiform chromite deposits in ophiolites: Implications of Re–Os systematics in the Dongqiao Neo-tethyan ophiolite, northern Tibet. *Gondwana Res.* 21 (1), 194–206.

Shojaat, B., 1999. Applications of Geochemical Models for Determining Tectonic Environment and Potential for Ore Deposits in Sabzevar Ophiolite, North Central Iran. PhD (Geol.) Dissertation. Azad Univ., Tehran.

Stampfli, G.M., 1978. Etude géologique générale de l'Elbourz oriental au sud de Gonbad-e-Qabus (Iran, NE). PhD Thesis. Univ. de Genève.

Stampfli, G.M., Borel, G.D., 2002. A plate tectonic model for the Paleozoic and Mesozoic constrained by dynamic plate boundaries and restored synthetic oceanic isochrons. *Earth Planet. Sci. Lett.* 196, 17–33.

Stampfli, G.M., Marcoux, J., Baud, A., 1991. Tethyan margins in space and time. *Palaeogeogr. Palaeoclimatol. Palaeoecol.* 87, 373–409.

Stille, P., Unruh, D.M., Tatsumoto, M., 1983. Pb, Sr, Nd, and Hf isotopic evidence of multiple sources for Oahu, Hawaii basalts. *Nature* 304, 25–29.

Stöcklin, J., 1968. Structural history and tectonics of Iran: a review. *AAPG Bull.* 52 (7), 1229–1258.

Stöcklin, J., 1974. Possible ancient continental margins in Iran, in: Burk, C.A., Drake, C.L. (Eds.), *The Geology of Continental Margins*. Springer, New York, pp. 873–887.

Stracke, A., Bizimis, M., Salters, V.J.M., 2003. Recycling oceanic crust: Quantitative constraints. *Geochem. Geophys. Geosyst.* 4 (3), 8003.

Sun, S.S., McDonough, W.F., 1989. Chemical and isotopic systematics of oceanic basalts: Implications for mantle composition and processes, in: Saunders, A.D., Norry, M.J. (Eds.), *Magmatism in Ocean Basins*. *Geol. Soc. London Spec. Publ.* 42 (1), 313–345.

Takin, M., 1972. Iranian geology and continental drift in the Middle East. *Nature* 235, 147–150.

Taylor, P.N., Jones, N.W., Moorbath, S., 1984. Isotopic assessment of relative contributions from crust and mantle sources to magma genesis of Precambrian granitoid rocks. *Phil. Trans. R. Soc. London A310*, 605–625.

Treloar, P.J., Mayringer, F., Finger, F., Gerdes, A., Shengelia, D., 2009. New age data from the Dzirula Massif, Georgia: implications for Variscan evolution of the Caucasus. 2nd Int. Symp. on the Geology of the Black Sea Region, Abstract Book, pp. 204–205.

Tucker, P.J., Hassanipak, A.A., Spell, T.L., Ghazi, A.M., 2000. Geochemistry, petrology and $^{40}\text{Ar}/^{39}\text{Ar}$ ages of the Shahr-e-Babak ophiolite, Central Iran. *EOS (Trans. AGU)* 80, F1095.

Weaver, B.L., 1991. The origin of ocean island basalt end-member compositions: Trace element and isotopic constraints. *Earth Planet. Sci. Lett.* 104, 381–397, doi: 10.1016/0012-821X(91)90217-6.

Wood, D.A., 1980. The application of a Th–Hf–Ta diagram to problems of tectonomagmatic classification and to establishing the nature of crustal contamination of basaltic lavas of the British Tertiary volcanic province. *Earth Planet. Sci. Lett.* 50 (1), 11–30.

Zakariadze, G.S., Dilek, Y., Adamia, S.A., Oberhänsli, R.E., Karpenko, S.F., Bazylev, B.A., Solov'eva, N., 2007. Geochemistry and geochronology of the Neoproterozoic Pan-African Transcaucasian Massif (Republic of Georgia) and implications for island arc evolution of the late Precambrian Arabian–Nubian Shield. *Gondwana Res.* 11 (1–2), 92–108.

Zanchetta, S., Zanchi, A., Villa, I., Poli, S., Muttoni, G., 2009. The Shanderman eclogites: A Late Carboniferous high-pressure event in the NW Talesh Mountains (NW Iran), in: Brunet, M.-F., Wilmsen, M., Granath, J.W. (Eds.), *South Caspian to Central Iran Basins*. *Geol. Soc. London Spec. Publ.* 312 (1), 57–78.

Zanchetta, S., Berra, F., Zanchi, A., Bergomi, M., Caridroit, M., Nicora, A., Heidarzadeh, G., 2013. The record of the Late Palaeozoic active margin of the Palaeotethys in NE Iran: Constraints on the Cimmerian orogeny. *Gondwana Res.* 24, 1237–1266.

Zanchi, A., Zanchetta, S., Berra, F., Mattei, M., Garzanti, E., Molyneux, S., Nawab, A., Sabouri, J., 2009. The Eo-Cimmerian (Late? Triassic) orogeny in north Iran, in: Brunet, M.-F., Wilmsen, M., Granath, J.W. (Eds.), *South Caspian to Central Iran Basins*. *Geol. Soc. London Spec. Publ.* 312 (1), 31–55.

Zhai, Q.G., Jahn, B.M., Wang, J., Su, L., Mo, X.X., Wang, K.L., Tang, S.H., Lee, H.Y., 2013. The Carboniferous ophiolite in the middle of the Qiangtang terrane, Northern Tibet: SHRIMP U–Pb dating, geochemical and Sr–Nd–Hf isotopic characteristics. *Lithos* 168–169, 186–199.

Zindler, A., Hart, S.R., 1986. Chemical geodynamics. *Annu. Rev. Earth Planet. Sci.* 14, 493–571.

Zonenshain, L.P., Kuzmin, M.I., Natapov, L.M., 1990. *Geology of the USSR: a plate-tectonic synthesis*. AGU, *Geodyn. Ser.* 21.

*Поступила в редакцию 10 августа 2019 г.,
принята в печать 28 февраля 2020 г.*